

Fast boundary integral method for acoustic wave scattering in two-dimensional layered media

Linfeng Xia^a, Heng Yuan^a, Bo Wang^{a,b,*}, Wei Cai^c

^a*LCSM, Ministry of Education, School of Mathematics and Statistics, Hunan Normal University, Changsha, Hunan 410081, P. R. China.*

^b*Xiangjiang Laboratory, Changsha, 410205, P. R. China.*

^c*Department of Mathematics, Southern Methodist University, Dallas, TX 75275, USA.*

Abstract

In this paper, we present a fast boundary integral method accelerated by the fast multipole method (FMM) for acoustic wave scattering governed by the scalar Helmholtz equation in multi-layered two-dimensional media. Multiple scatterers are randomly distributed in the multi-layered medium with some scatterers possibly intersecting layer interfaces. The boundary integral formulation employs a layered-medium Green's function to enforce transmission conditions across interfaces, thus avoiding unknowns on the interfaces and significantly reducing the size of the discretized problem compared to approaches that use a free-space Green's function. To demonstrate the FMM speedup, a low-order Nyström method is used to discretize the boundary integral equation and then the resulting dense linear system is solved by GMRES iterative solver accelerated by an improved layered media FMM and a overlapping domain decomposition preconditioning. In the low frequency regime, the proposed algorithm achieves an $\mathcal{O}(N)$ complexity. Numerical results validate the accuracy, efficiency, and robustness of the method under complex settings and various incident angles. The proposed framework provides a scalable and efficient solver for acoustic wave scattering in layered media.

Keywords: Multiple scattering, layered media, Nyström method, fast multipole method, GMRES iteration.

1. Introduction

Wave scattering in layered media is a fundamental problem in acoustics [1], electromagnetics, and geophysics [2], with a wide range of applications from subsurface imaging to antenna design [3] and optical waveguide analysis. The governing model is the Helmholtz equation posed in piecewise homogeneous domains separated by planar or curved interfaces, where continuity conditions across the interfaces must be enforced. Numerical simulations of such problems are notoriously challenging. Traditional domain-based discretization methods, such as the finite element method (FEM) or the finite difference method (FDM), require the introduction of artificial truncation boundaries to approximate the unbounded physical domain, typically combined with techniques such as perfectly matched layers (PML) [4, 5, 6, 7] or absorbing boundary conditions (ABCs) [8, 9, 10, 11]. While these approaches are highly versatile, they generally lead to very large linear systems, particularly in high-frequency regimes,

*Corresponding author

Email address: bowang@hunnu.edu.cn (Bo Wang)

rendering large-scale computations prohibitively expensive. Moreover, the construction of the ABCs and the stability of the PML technique for multi-layered media are still challenging.

Boundary integral equation (BIE) methods [12, 13, 14, 15] provide an attractive alternative to address these challenges. By using Green's functions, BIE reformulates the governing partial differential equations into integral equations posed solely on the boundary of the scatterer. This approach offers significant advantages of dimensional reduction, which greatly reduces the number of unknowns. Furthermore, BIE methods inherently enforce the radiation condition at infinity, eliminating the need for artificial domain truncation and thus avoiding the need of PML-type or ABCs techniques. These properties make BIE methods especially suitable for exterior scattering problems.

Despite these intrinsic advantages, the application of BIEs to layered media with complex and multiscale structures encounters two principal computational bottlenecks. First, the Nyström discretization results in dense and typically non-symmetric linear system. For a problem with N unknowns, classical direct solvers (e.g., Gaussian elimination) entail both storage and computational complexities of order $O(N^3)$, which is prohibitively expensive for problems with large numbers of unknowns. Second, the evaluation of layered Green's functions is itself highly challenging, as they are represented by Sommerfeld integrals [16, 17] with oscillatory and slowly decaying kernels, often requiring the numerical computation of semi-infinite integrals significantly more expensive than the evaluation of free-space Green's functions.

To address the first bottleneck associated with dense linear system, a broad spectrum of fast algorithms has been developed over the past three decades. For instance, Hackbusch and collaborators introduced the hierarchical matrix (\mathcal{H} -matrix) framework [18], which leverages block-wise low-rank approximations to construct data-sparse representations, enabling fast matrix–vector multiplications, approximate LU factorization, and direct solvers. Bebendorf and co-workers further developed adaptive cross approximation (ACA) and block low-rank methods [19], which construct low-rank representations adaptively from a small number of row and column samples, significantly reducing assembly and storage costs. Additional progress includes Fourier integral operator (FIO)-oriented methods suitable for high-frequency regimes [20], as well as recursive skeletonization and other fast direct solvers designed for problems with multiple right-hand sides or highly ill-conditioned systems [21, 22]. Among these, the fast multipole method (FMM) introduced by Greengard and Rokhlin [23] stands out for its remarkable efficiency: by hierarchically compressing far-field interactions via multipole and local expansions, it reduces the cost of matrix–vector multiplications from $O(N^2)$ to nearly linear complexity ($O(N)$ or $O(N \log N)$). Subsequent extensions have adapted FMM to BIEs [24] and layered media FMMs [25], thereby retaining scalability while effectively accounting for interface reflections and transmissions.

Applying these fast algorithms to layered media scattering problems introduces the second major bottleneck: the expensive evaluation of layered Green's functions. Early techniques include the discrete complex image method (DCIM) and contour deformation approaches, but both face substantial limitations for multilayered configurations. To address these challenges, Cai and Yu developed a window-based acceleration strategy [26] to mitigate the slow convergence of the Sommerfeld integrals caused by surface-wave poles, the slow decay of spectral Green's functions, and oscillations in Hankel-transform kernels. Michalski and Mosig later provided a comprehensive review of efficient evaluation strategies for the Sommerfeld integrals [27], focusing on handling the oscillatory and singular behaviors of layered kernels. More recent advances have introduced even more efficient and robust methods, including the windowed Green's function (WGF) method [28], the PML-BIE method [29, 30, 31], hybrid integral formulations [32], and numerical quadratures of high-accuracy such as the Tanh–Sinh quadrature for Sommerfeld-type integrals [33].

In this work, we investigate the two-dimensional acoustic wave scattering problem in multilayered media and propose a fast boundary integral method accelerated by FMM for layered Green's function of the Helmholtz equation. First, We derive the layered Green's function that satisfies the transmission conditions across all interfaces, which allows the resulting boundary integral formulation to substantially reduce the number of unknowns. Secondly, building on the FMM developed for the Helmholtz equation in layered media [34, 25], we improve the two-dimensional setting with an enhancement of equivalent polarization coordinate and effective location techniques proposed in [35]. Specifically, we give an more accurate description of the vertical transmission distance of the reaction-field components and employ polarization coordinates for sources as well as effective locations for targets, thereby improving both the accuracy and efficiency of the FMM. With FMM acceleration, the solution of linear systems arising from low-order Nyström discretizations achieves nearly linear computational complexity, enabling efficient simulation of large-scale problems. Furthermore, inspired by the preconditioner based on the hierarchical tree structure of the FMM (cf. [36]), we develop an effective preconditioning strategy that mitigates the deterioration of the system's condition number as the problem size increases, reducing both the iteration count and the computational time by roughly one half. Extensive numerical experiments demonstrate that the proposed method is accurate, robust, and highly efficient, achieving nearly linear computational complexity while maintaining first-order numerical accuracy.

The remainder of the paper is organized as follows. In Section 2, we formulate the two-dimensional Helmholtz scattering problem in a multi-layered medium with a plane incident wave from the top layer. By splitting out the background scattering field, an interface problem for the purely outgoing wave is formulated. Then, a boundary integral method with Nyström discretization is presented in Section 3. Here, we use the layered Green's function to naturally impose transmission conditions without introducing redundant unknowns on the interface. In Section 4, an improved fast multipole algorithm is proposed to accelerate the matrix-vector product in the GMRES iterative algorithm and an overlapping domain decomposition preconditioner is presented based on the tree structure of the FMM to reduce the number of iterations. In Section 5, numerical examples with multiple scatterers randomly distributed in multi-layered media are provided to validate the accuracy and efficiency of the proposed algorithm.

2. Acoustic wave scattering problem in two-dimensional layered media

2.1. Model problem

Consider the layered media of $L + 1$ layers with interfaces $y = -d_\ell$, $\ell = 0, 1, \dots, L - 1$ and reflection index $\{\eta_\ell\}_{\ell=0}^L$. Let $\{D_j\}_{j=1}^M$ be M impenetrable scatterers randomly distributed in the layered media and $\{\partial D_j\}_{j=1}^M$ define the boundaries of scatterers $\{D_j\}_{j=1}^M$. Each of the scatterers can be located in one layer or cross multiple layers, see Fig. 2.1. Denote by

$$\begin{aligned} \Upsilon_0 &= \{(x, y) | y > -d_0\}, & \Upsilon_L &= \{(x, y) | y < -d_{L-1}\}, \\ \Upsilon_\ell &= \{(x, y) | -d_\ell < y < -d_{\ell-1}\}, & \ell &= 1, 2, \dots, L - 1, \end{aligned} \quad (2.1)$$

the infinite strips of the layers,

$$\Omega_\ell = \bigcup_{i=1}^M \Omega_i^{(\ell)} = \bigcup_{i=1}^M (\Upsilon_\ell \cap D_i), \quad \ell = 0, 1, \dots, L, \quad (2.2)$$

the disconnected domains in the ℓ -th layer occupied by the multiple scatterers, and

$$\Gamma_\ell = \bigcup_{i=1}^M \Gamma_i^{(\ell)} = \bigcup_{i=1}^M (\Upsilon_\ell \cap \partial D_i), \quad \ell = 0, 1, \dots, L, \quad (2.3)$$

the boundary of the disconnected domain.

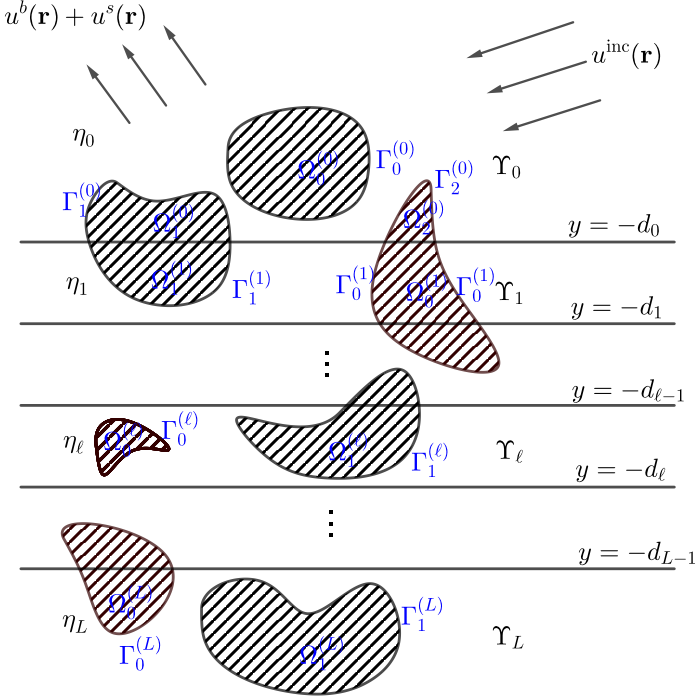


Figure 2.1: Configurations of the scattering problem in layered media.

The mathematical model of a time-harmonic acoustic scattering problem under this general setting is the Helmholtz equation of the form

$$(\Delta + k_\ell^2)u(\mathbf{r}) = 0, \quad \mathbf{r} \in \Upsilon_\ell \setminus \Omega_\ell, \quad \ell = 0, 1, \dots, L, \quad (2.4)$$

in each layer. Here, $u = u^{\text{sc}}(\mathbf{r}) + u^{\text{inc}}(\mathbf{r})$ is the total field, k_ℓ is the wave number in the ℓ -th layer. The incident wave $u^{\text{inc}}(\mathbf{r})$ is typically a plane wave given in the 0-th layer. Its expression is given by

$$u^{\text{inc}}(\mathbf{r}) = \begin{cases} e^{i(k_{0,x}x - k_{0,y}y)}, & y > -d_0, \\ 0, & \text{otherwise,} \end{cases} \quad (2.5)$$

where $(k_{0,x}, k_{0,y})$ is the propagating vector such that $k_{0,y} > 0$, and $(k_{0,x})^2 + (k_{0,y})^2 = k_0^2$. Due to the presence of the layered media, transmission conditions

$$[u] = 0, \quad \left[\eta \frac{\partial u}{\partial \mathbf{n}} \right] = 0, \quad y = -d_\ell, \quad \ell = 0, 1, \dots, L-1, \quad (2.6)$$

are imposed on the interfaces. On the boundaries of the scatterers, the Dirichlet, Neumann or Robin boundary conditions could be imposed according to different materials of the scatterers. For simplicity of presentation, only sound soft (Dirichlet) boundary condition, i.e,

$$u(\mathbf{r}) = 0, \quad \mathbf{r} \in \Omega_\ell, \quad \ell = 0, 1, \dots, L \quad (2.7)$$

will be considered in this paper.

2.2. Background scattering field

The reflection of plane waves by a layered structure can be calculated analytically. In order to formulate BIEs for the scattering problem, we separate the background scattering field from the scattering field $u^{sc}(\mathbf{r})$. The background scattering field denoted by $u^b(\mathbf{r})$ is the reflected fields within the layered media in the absence of scatterers. It satisfies

$$\begin{aligned} (\Delta + k_\ell^2)u^b(\mathbf{r}) &= 0, \quad \mathbf{r} \in \Upsilon_\ell, \quad \ell = 0, 1, \dots, L, \\ \llbracket u^b + u^{\text{inc}} \rrbracket &= 0, \quad \left[\eta \left(\frac{\partial u^b}{\partial \mathbf{n}} + \frac{\partial u^{\text{inc}}}{\partial \mathbf{n}} \right) \right] = 0, \quad y = -d_0, \\ \llbracket u^b \rrbracket &= 0, \quad \left[\eta \frac{\partial u^b}{\partial \mathbf{n}} \right] = 0, \quad y = -d_\ell, \quad \ell = 1, \dots, L-1, \end{aligned} \quad (2.8)$$

it is well-known that $u^b(\mathbf{r})$ has an ansatz expression

$$u^b(\mathbf{r}) = \begin{cases} A_0 e^{i(k_{0,x}x + k_{0,y}y)}, & \mathbf{r} \in \Upsilon_0, \\ A_\ell e^{i(k_{\ell,x}x + k_{\ell,y}y)} + B_\ell e^{i(k_{\ell,x}x - k_{\ell,y}y)}, & \mathbf{r} \in \Upsilon_\ell, \quad \ell \neq 0, L, \\ B_L e^{i(k_{L,x}x - k_{L,y}y)}, & \mathbf{r} \in \Upsilon_L. \end{cases} \quad (2.9)$$

Applying the interface conditions gives

$$\begin{aligned} k_{L,x} &= k_{L-1,x} = \dots = k_{1,x} = k_{0,x}, \quad k_{\ell,y} = \sqrt{k_\ell^2 - k_{\ell,x}^2}, \\ A_0 &= \tilde{R}_{01} e^{2ik_{0,y}d_0}, \quad B_L = \tilde{T}_{0L}, \\ A_\ell &= \tilde{R}_{\ell\ell+1} \tilde{T}_{0\ell} e^{2ik_{\ell,y}d_\ell}, \quad B_\ell = \tilde{T}_{0\ell}, \quad \ell = 1, 2, \dots, L-1, \end{aligned} \quad (2.10)$$

where the general reflection coefficients $\{\tilde{R}_{\ell\ell+1}(\lambda)\}_{\ell=0}^{L-1}$ and general transmission coefficients $\{\tilde{T}_{0\ell}(\lambda)\}_{\ell=1}^L$ are defined in (3.5) and (3.6), respectively.

Then, the scattering field due to the presence of the scatterers is defined as

$$u^s(\mathbf{r}) = u(\mathbf{r}) - u^b(\mathbf{r}) - u^{\text{inc}}(\mathbf{r}),$$

which is the solution of the following scattering problem

$$\begin{aligned} (\Delta + k_\ell^2)u^s(\mathbf{r}) &= 0, \quad \mathbf{r} \in \Upsilon_\ell \setminus \Omega_\ell, \quad \ell = 0, 1, \dots, L, \\ u^s(\mathbf{r}) &= g(\mathbf{r}), \quad \mathbf{r} \in \Gamma_\ell, \quad \ell = 0, 1, \dots, L, \\ \llbracket u^s \rrbracket &= 0, \quad \left[\eta \frac{\partial u^s}{\partial \mathbf{n}} \right] = 0, \quad y = -d_\ell, \quad \ell = 0, 1, \dots, L-1, \\ u^s(\mathbf{r}) &\text{ is outing as } |\mathbf{r}| \rightarrow \infty. \end{aligned} \quad (2.11)$$

Here, the boundary data is given by

$$g(\mathbf{r}) = \begin{cases} -u^{\text{inc}}(\mathbf{r}) - u^b(\mathbf{r}), & \mathbf{r} \in \Gamma_0, \\ -u^b(\mathbf{r}), & \mathbf{r} \in \bigcup_{\ell=1}^L \Gamma_\ell, \end{cases} \quad (2.12)$$

which implies that the actual incident wave is the superposition of the original incident wave and the background scattering wave. In the rest of this paper, we will employ the boundary integral technique to develop a fast algorithm to solve the wave scattering problem (2.11).

3. Boundary integral equation and Nyström discretization

In this section, we employ the layered Green's function (3.8) to derive BIEs for the model problem (2.11) and then develop a fast numerical algorithm based on Nyström discretization and FMM accelerated GMRES solver. Due to the use of layered Green's function, The transmission interface conditions are automatically satisfied by the integral representation of the solution and the integral equation is formulated solely on the boundaries of the scatterers.

3.1. Green's function of the Helmholtz equation in layered media

Suppose we have a point source at $\mathbf{r}' = (x', y')$ in the ℓ' th layer ($-d_{\ell'} < y' < -d_{\ell'-1}$) of the layered medium depicted in Fig. 2.1, the layered media Green's function $u_{\ell\ell'}(\mathbf{r}, \mathbf{r}')$ for Helmholtz equation satisfies

$$(\Delta + k_\ell^2)G_{\ell\ell'}(\mathbf{r}, \mathbf{r}') = -\delta(\mathbf{r}, \mathbf{r}'), \quad (3.1)$$

at field point $\mathbf{r} = (x, y)$ in the ℓ th layer ($-d_\ell < y < -d_{\ell-1}$) where $\delta(\mathbf{r}, \mathbf{r}')$ is the Dirac delta function.

For any $\ell = 0 \rightarrow L-1$, the reflection and transmission coefficients due to the interface $y = -d_\ell$ are given by

$$R_{\ell\ell+1}(\lambda) = \frac{\eta_\ell k_{\ell,y} - \eta_{\ell+1} k_{\ell+1,y}}{\eta_\ell k_{\ell,y} + \eta_{\ell+1} k_{\ell+1,y}}, \quad T_{\ell\ell+1}(\lambda) = \frac{2\eta_\ell k_{\ell,y}}{\eta_\ell k_{\ell,y} + \eta_{\ell+1} k_{\ell+1,y}}, \quad (3.2)$$

if a plane wave $e^{i(\lambda x + k_{\ell,y} y)}$ is incident from above. In contrast, if a plane wave $e^{i(\lambda x + k_{\ell+1,y} y)}$ is incident from the $(\ell+1)$ -th layer from below, the reflection and transmission coefficients are

$$R_{\ell+1,\ell} = -R_{\ell\ell+1}, \quad T_{\ell+1,\ell} = \frac{\eta_{\ell+1} k_{\ell+1,y}}{\eta_\ell k_{\ell,y}} T_{\ell\ell+1}. \quad (3.3)$$

In order to investigate the multi-layered problem, the general reflection and transmission coefficients were introduced (cf. [37]). Two groups of general reflection coefficients $\{\tilde{R}_{\ell+1,\ell}(\lambda)\}_{\ell=0}^{L-1}$, $\{\tilde{R}_{\ell\ell+1}(\lambda)\}_{\ell=0}^{L-1}$ can be calculated via two recursions as follows

- Set $\tilde{R}_{0,-1}(\lambda) = 0$, then

$$\tilde{R}_{\ell+1,\ell}(\lambda) = \frac{R_{\ell+1,\ell} + \tilde{R}_{\ell\ell-1}(\lambda)e^{-2k_{\ell,y}(d_\ell - d_{\ell-1})}}{1 + R_{\ell+1,\ell}\tilde{R}_{\ell\ell-1}(\lambda)e^{-2k_{\ell,y}(d_\ell - d_{\ell-1})}}, \quad \ell = 0, 1, \dots, L-1. \quad (3.4)$$

- Set $\tilde{R}_{L-1,L}(\lambda) = 0$, then

$$\tilde{R}_{\ell\ell+1}(\lambda) = \frac{R_{\ell\ell+1} + \tilde{R}_{\ell+1,\ell+2}(\lambda)e^{-2k_{\ell+1,y}(d_{\ell+1} - d_\ell)}}{1 + R_{\ell\ell+1}\tilde{R}_{\ell+1,\ell+2}(\lambda)e^{-2k_{\ell+1,y}(d_{\ell+1} - d_\ell)}}, \quad \ell = L-2, L-3, \dots, 0. \quad (3.5)$$

The general transmission coefficient from ℓ' -th layer to ℓ -th layer has recursion

$$\tilde{T}_{\ell'\ell}(\lambda) = \begin{cases} \frac{T_{\ell+1,\ell}(\lambda)e^{i(k_{\ell,y} - k_{\ell+1,y})d_\ell}\tilde{T}_{\ell'\ell+1}(\lambda)}{1 + R_{\ell+1,\ell}(\lambda)\tilde{R}_{\ell,\ell-1}(\lambda)e^{-2k_{\ell,y}(d_\ell - d_{\ell-1})}}, & \ell = \ell' - 1, \ell' - 2, \dots, 0, \\ \frac{T_{\ell-1,\ell}(\lambda)e^{i(k_{\ell-1,y} - k_{\ell,y})d_{\ell-1}}\tilde{T}_{\ell'\ell-1}(\lambda)}{1 + R_{\ell-1,\ell}(\lambda)\tilde{R}_{\ell,\ell+1}(\lambda)e^{-2k_{\ell,y}(d_\ell - d_{\ell-1})}}, & \ell = \ell' + 1, \ell' + 2, \dots, L, \end{cases} \quad (3.6)$$

where the initial value is given by $\tilde{T}_{\ell'\ell'}(\lambda) \equiv 1$.

By using Fourier transforms along x -directions, the problem (3.1) can be solved analytically for each layer in y by imposing transmission conditions at the interface between ℓ th and $(\ell-1)$ th layer ($y = -d_{\ell-1}$), *i.e.*,

$$G_{\ell-1,\ell'}(\mathbf{r}, \mathbf{r}') = G_{\ell\ell'}(\mathbf{r}, \mathbf{r}'), \quad \eta_{\ell-1} \frac{\partial G_{\ell-1,\ell'}(\mathbf{r}, \mathbf{r}')}{\partial y} = \eta_\ell \frac{\partial G_{\ell\ell'}(\mathbf{r}, \mathbf{r}')}{\partial y}, \quad (3.7)$$

as well as the outgoing conditions in the top and bottom-most layers as $y \rightarrow \pm\infty$. Here, we just present the expression of the layered Green's function. Detailed derivation can be found in (cf. [37, 38]). The expression of the Green's function in the physical domain takes the form

$$G_{\ell\ell'}(\mathbf{r}, \mathbf{r}') = \delta_{\ell\ell'} G_{\ell}^f(\mathbf{r}, \mathbf{r}') + G_{\ell\ell'}^r(\mathbf{r}, \mathbf{r}'), \quad (3.8)$$

where $\delta_{\ell\ell'}$ is the Kronecker symbol,

$$G_{\ell}^f(\mathbf{r}, \mathbf{r}') = \frac{i}{4} H_0^{(1)}(k_{\ell} |\mathbf{r} - \mathbf{r}'|) \quad (3.9)$$

is the free space Green's function with wave number k_{ℓ} , $G_{\ell\ell'}^r(\mathbf{r}, \mathbf{r}')$ is the reaction component. In general, $G_{\ell\ell'}^r(\mathbf{r}, \mathbf{r}')$ does not have closed form. It is usually given by the inverse Fourier transform of the Green's function in the spectral domain. According to the dependence on the y and y' coordinates, the reaction component $G_{\ell\ell'}^r(\mathbf{r}, \mathbf{r}')$ generally consists of four components, i.e.,

$$G_{\ell\ell'}^r(\mathbf{r}, \mathbf{r}') = G_{\ell\ell'}^{\uparrow\downarrow}(\mathbf{r}, \mathbf{r}') + G_{\ell\ell'}^{\uparrow\uparrow}(\mathbf{r}, \mathbf{r}') + G_{\ell\ell'}^{\downarrow\downarrow}(\mathbf{r}, \mathbf{r}') + G_{\ell\ell'}^{\downarrow\uparrow}(\mathbf{r}, \mathbf{r}'), \quad (3.10)$$

where

$$\begin{aligned} G_{\ell\ell'}^{\uparrow\downarrow}(\mathbf{r}, \mathbf{r}') &= \begin{cases} \frac{1}{2\pi} \int_{-\infty}^{\infty} \frac{e^{i\lambda(x-x') + i(k_{\ell,y}y - k_{\ell',y}\tau_{\ell'}(y'))}}{2k_{\ell',y}} \sigma_{\ell\ell'}^{\uparrow\downarrow}(\lambda) d\lambda, & 0 \leq \ell \leq \ell', \\ \frac{1}{2\pi} \int_{-\infty}^{\infty} \frac{e^{i\lambda(x-x') + i(k_{\ell',y}y' - k_{\ell,y}\tau_{\ell}(y))}}{2k_{\ell',y}} \sigma_{\ell\ell'}^{\uparrow\downarrow}(\lambda) d\lambda, & \ell' < \ell \leq L, \end{cases} \\ G_{\ell\ell'}^{\uparrow\uparrow}(\mathbf{r}, \mathbf{r}') &= \begin{cases} \frac{1}{2\pi} \int_{-\infty}^{\infty} \frac{e^{i\lambda(x-x') + i(k_{\ell,y}y - k_{\ell',y}y')}}{2k_{\ell',y}} \sigma_{\ell\ell'}^{\uparrow\uparrow}(\lambda) d\lambda, & 0 \leq \ell < \ell', \\ \frac{1}{2\pi} \int_{-\infty}^{\infty} \frac{e^{i\lambda(x-x') + i(k_{\ell',y}\tau_{\ell'-1}(y') - k_{\ell,y}\tau_{\ell}(y))}}{2k_{\ell',y}} \sigma_{\ell\ell'}^{\uparrow\uparrow}(\lambda) d\lambda, & \ell' \leq \ell \leq L, \end{cases} \\ G_{\ell\ell'}^{\downarrow\downarrow}(\mathbf{r}, \mathbf{r}') &= \begin{cases} \frac{1}{2\pi} \int_{-\infty}^{\infty} \frac{e^{i\lambda(x-x') + i(k_{\ell,y}\tau_{\ell-1}(y) - k_{\ell',y}\tau_{\ell'}(y'))}}{2k_{\ell',y}} \sigma_{\ell\ell'}^{\downarrow\downarrow}(\lambda) d\lambda, & 0 \leq \ell \leq \ell', \\ \frac{1}{2\pi} \int_{-\infty}^{\infty} \frac{e^{i\lambda(x-x') + i(k_{\ell',y}y' - k_{\ell,y}y)}}{2k_{\ell',y}} \sigma_{\ell\ell'}^{\downarrow\downarrow}(\lambda) d\lambda, & \ell' < \ell \leq L, \end{cases} \\ G_{\ell\ell'}^{\downarrow\uparrow}(\mathbf{r}, \mathbf{r}') &= \begin{cases} \frac{1}{2\pi} \int_{-\infty}^{\infty} \frac{e^{i\lambda(x-x') + i(k_{\ell,y}\tau_{\ell-1}(y) - k_{\ell',y}y')}}{2k_{\ell',y}} \sigma_{\ell\ell'}^{\downarrow\uparrow}(\lambda) d\lambda, & 0 \leq \ell < \ell', \\ \frac{1}{2\pi} \int_{-\infty}^{\infty} \frac{e^{i\lambda(x-x') + i(k_{\ell',y}\tau_{\ell'-1}(y') - k_{\ell,y}y)}}{2k_{\ell',y}} \sigma_{\ell\ell'}^{\downarrow\uparrow}(\lambda) d\lambda, & \ell' \leq \ell \leq L. \end{cases} \end{aligned} \quad (3.11)$$

In the above integral representations,

$$\tau_m(a) = -2d_m - a, \quad m = 0, 1, \dots, L-1 \quad (3.12)$$

are the reflection of any given a according to the interface $y = -d_m$, and the densities are given by

• **Case I:** $\ell = \ell'$,

$$\begin{aligned} \sigma_{\ell'\ell'}^{\uparrow\downarrow}(\lambda) &= \frac{\tilde{R}_{\ell'\ell'+1}}{1 - \tilde{R}_{\ell\ell+1}\tilde{R}_{\ell\ell-1}e^{-2k_{\ell',y}(d_{\ell'} - d_{\ell'-1})}}, \\ \sigma_{\ell'\ell'}^{\downarrow\uparrow}(\lambda) &= \frac{\tilde{R}_{\ell'\ell'-1}}{1 - \tilde{R}_{\ell\ell+1}\tilde{R}_{\ell\ell-1}e^{-2k_{\ell',y}(d_{\ell'} - d_{\ell'-1})}}, \\ \sigma_{\ell'\ell'}^{\uparrow\uparrow}(\lambda) &= \sigma_{\ell'\ell'}^{\downarrow\downarrow}(\lambda) = \tilde{R}_{\ell'\ell'-1}\sigma_{\ell\ell'}^{\uparrow\downarrow}(\lambda) = \tilde{R}_{\ell'\ell'+1}\sigma_{\ell\ell'}^{\downarrow\uparrow}(\lambda). \end{aligned} \quad (3.13)$$

- **Case II:** $0 \leq \ell < \ell'$,

$$\begin{aligned}\sigma_{\ell\ell'}^{\downarrow\downarrow}(\lambda) &= \tilde{T}_{\ell'\ell}(\lambda)\sigma_{\ell'\ell'}^{\downarrow\downarrow}(\lambda), & \sigma_{\ell\ell'}^{\uparrow\uparrow}(\lambda) &= \tilde{T}_{\ell'\ell}(\lambda)\left[1 + \sigma_{\ell'\ell'}^{\uparrow\uparrow}(\lambda)e^{2ik_{\ell',y}(d_{\ell'} - d_{\ell'-1})}\right], \\ \sigma_{\ell\ell'}^{\downarrow\uparrow}(\lambda) &= \tilde{R}_{\ell\ell-1}(\lambda)\sigma_{\ell\ell'}^{\downarrow\downarrow}(\lambda), & \sigma_{\ell\ell'}^{\downarrow\uparrow}(\lambda) &= \tilde{R}_{\ell\ell-1}(\lambda)\sigma_{\ell\ell'}^{\uparrow\uparrow}(\lambda).\end{aligned}\quad (3.14)$$

- **Case III:** $\ell' < \ell \leq L$

$$\begin{aligned}\sigma_{\ell\ell'}^{\downarrow\uparrow}(\lambda) &= \tilde{T}_{\ell'\ell}(\lambda)\sigma_{\ell'\ell'}^{\downarrow\uparrow}(\lambda), & \sigma_{\ell\ell'}^{\downarrow\downarrow}(\lambda) &= \tilde{T}_{\ell'\ell}(\lambda)\left[1 + \sigma_{\ell'\ell'}^{\downarrow\downarrow}(\lambda)e^{2ik_{\ell',y}(d_{\ell'} - d_{\ell'-1})}\right], \\ \sigma_{\ell\ell'}^{\uparrow\uparrow}(\lambda) &= \tilde{R}_{\ell\ell+1}(\lambda)\sigma_{\ell\ell'}^{\downarrow\uparrow}(\lambda), & \sigma_{\ell\ell'}^{\uparrow\downarrow}(\lambda) &= \tilde{R}_{\ell\ell+1}(\lambda)\sigma_{\ell\ell'}^{\downarrow\downarrow}(\lambda).\end{aligned}\quad (3.15)$$

As in our previous work [35], we introduce the *equivalent polarization coordinates*

$$\check{\tau}_{\ell\ell'}(\mathbf{r}') = \begin{cases} \tau_{\ell'}(\mathbf{r}'), & \ell \leq \ell', \\ \mathbf{r}', & \ell > \ell', \end{cases} \quad \check{\tau}_{\ell\ell'}^{\uparrow}(\mathbf{r}') = \begin{cases} \mathbf{r}', & \ell < \ell', \\ \tau_{\ell'-1}(\mathbf{r}'), & \ell \geq \ell', \end{cases} \quad (3.16)$$

for source \mathbf{r}' and *effective locations*

$$\begin{aligned}\hat{\tau}_{\ell\ell'}^{\uparrow\uparrow}(\mathbf{r}) &= \begin{cases} \mathbf{r}, & \ell < \ell', \\ \tau_{\ell}(\mathbf{r}), & \ell \geq \ell', \end{cases} & \hat{\tau}_{\ell\ell'}^{\downarrow\downarrow}(\mathbf{r}) &= \begin{cases} \mathbf{r}, & \ell \leq \ell', \\ \tau_{\ell}(\mathbf{r}), & \ell > \ell', \end{cases} \\ \hat{\tau}_{\ell\ell'}^{\downarrow\uparrow}(\mathbf{r}) &= \begin{cases} \tau_{\ell-1}(\mathbf{r}), & \ell < \ell', \\ \mathbf{r}, & \ell \geq \ell', \end{cases} & \hat{\tau}_{\ell\ell'}^{\uparrow\downarrow}(\mathbf{r}) &= \begin{cases} \tau_{\ell-1}(\mathbf{r}), & \ell \leq \ell', \\ \mathbf{r}, & \ell > \ell', \end{cases}\end{aligned}\quad (3.17)$$

for target \mathbf{r} with

$$\tau_{\ell}(\mathbf{r}) := (x, \tau_{\ell}(y)). \quad (3.18)$$

Then, the integral formulations for the reaction components $G_{\ell\ell'}^{**}$ can be written into the following uniform formulation

$$G_{\ell\ell'}^{**}(\mathbf{r}, \mathbf{r}') = \frac{1}{2\pi} \int_{-\infty}^{\infty} \frac{\mathcal{E}_{\ell\ell'}(\lambda, \hat{\tau}_{\ell\ell'}^{**}(\mathbf{r}), \check{\tau}_{\ell\ell'}^{*}(\mathbf{r}'))}{2k_{\ell',y}} \sigma_{\ell\ell'}^{**}(\lambda) d\lambda, \quad *, \star = \uparrow, \downarrow, \quad (3.19)$$

where

$$\mathcal{E}_{\ell\ell'}(\lambda, \mathbf{r}, \mathbf{r}') = e^{i\lambda(x-x') + \text{sgn}(y-y')(ik_{\ell,y}y - ik_{\ell',y}y')}.\quad (3.20)$$

Remark 3.1. Note that the general reflection coefficients $\tilde{R}_{\ell\ell'}(\lambda)$ in the top and bottom layers are defined as

$$\tilde{R}_{0,-1}(\lambda) = \tilde{R}_{L+1}(\lambda) \equiv 0.$$

Together with the formulas (3.14)-(3.15) imply that

$$\sigma_{0\ell'}^{\downarrow\downarrow}(\lambda) = \sigma_{0\ell'}^{\uparrow\uparrow}(\lambda) \equiv 0, \quad \sigma_{L\ell'}^{\uparrow\uparrow}(\lambda) = \sigma_{L\ell'}^{\downarrow\downarrow}(\lambda) \equiv 0, \quad \ell' = 0, 1, \dots, L.$$

On the other hand, the definition of $\sigma_{\ell'\ell'}^{**}(\lambda)$ in (3.13) implies that

$$\sigma_{00}^{\uparrow\uparrow}(\lambda) = \sigma_{00}^{\downarrow\uparrow}(k_{\rho}) = \sigma_{00}^{\downarrow\downarrow}(\lambda) \equiv 0, \quad \sigma_{LL}^{\uparrow\downarrow}(\lambda) = \sigma_{LL}^{\uparrow\uparrow}(k_{\rho}) = \sigma_{LL}^{\downarrow\downarrow}(\lambda) \equiv 0,$$

which further leads to

$$\sigma_{\ell 0}^{\uparrow\uparrow}(\lambda) = \sigma_{\ell 0}^{\downarrow\uparrow}(\lambda) = 0, \quad \sigma_{\ell L}^{\uparrow\downarrow}(\lambda) = \sigma_{\ell L}^{\downarrow\downarrow}(\lambda) = 0, \quad \ell = 0, 1, \dots, L,$$

due to the relations in (3.14) and (3.14). Thus, the following reaction components are zero

$$\begin{aligned}G_{0\ell'}^{\downarrow\downarrow}(\mathbf{r}, \mathbf{r}') &= G_{0\ell'}^{\downarrow\uparrow}(\mathbf{r}, \mathbf{r}') \equiv 0, & G_{L\ell'}^{\uparrow\uparrow}(\mathbf{r}, \mathbf{r}') &= G_{L\ell'}^{\uparrow\downarrow}(\mathbf{r}, \mathbf{r}') \equiv 0, \\ G_{\ell 0}^{\uparrow\uparrow}(\mathbf{r}, \mathbf{r}') &= G_{\ell 0}^{\downarrow\uparrow}(\mathbf{r}, \mathbf{r}') \equiv 0, & G_{\ell L}^{\uparrow\downarrow}(\mathbf{r}, \mathbf{r}') &= G_{\ell L}^{\downarrow\downarrow}(\mathbf{r}, \mathbf{r}') \equiv 0,\end{aligned}$$

for all $\ell, \ell' = 0, 1, \dots, L$. Therefore, the total number of non-zero reaction components is $4L^2$.

3.2. Effective transmission distance of reaction fields

In addition to the equivalent polarization coordinates proposed in our previous works [25, 34, 39], we introduce a new concept of effective location for the target particles, in order to account for the actual transmission distance of the reflected waves in layered media. The upward and downward waves generated by the source at \mathbf{r}' transmit to the target at \mathbf{r} via different paths, see Figs. 3.1 to 3.3, and generally induce upward and downward reaction fields. That is the physical background of the decomposition of four reaction field components. The reaction field decomposition (3.8) of Green's functions consists of the free space interaction provided $\ell = \ell'$, as well as the reaction field. When categorized by the upward/downward field propagation directions, the reaction field is decomposed into (up to) four terms in (3.11), each $\hat{G}_{\ell\ell'}^{**}$ representing one type with upward (\uparrow), downward (\downarrow) or both directions, with the first symbol $*$ indicating the direction of wave arriving at the target, and the second symbol $*$ indicating the direction of the wave leaving the source.

When the target and the source come from the same layer, i.e. $\ell = \ell'$, waves of the reaction field must have at least one reflection on interfaces due to the subtraction of the free-space part, see Fig. 3.1 for an illustration. For instance, the reaction field component $G_{\ell\ell'}^{\downarrow\downarrow}$ is interpreted as the superposition of waves that are downward at \mathbf{r}' and downward at \mathbf{r} , including the wave marked by the solid line with two reflections in Fig. 3.1(b), as well as any other contributions that may have experienced more reflections and transmissions on the interfaces. The minimal vertical transmission distance of these waves is given by the distance between the effective target location $\hat{\tau}_{\ell\ell'}^{\downarrow\downarrow}(\mathbf{r}) = \tau_{\ell'-1}(\mathbf{r})$ and the equivalent polarization source $\check{\tau}_{\ell\ell'}^{\downarrow}(\mathbf{r}') = \tau_{\ell'}(\mathbf{r}')$, as shown by the dashed line. Indeed, in the exponent of (3.20),

$$\mathcal{E}_{\ell\ell'}(\lambda, \hat{\tau}_{\ell\ell'}^{\downarrow\downarrow}(\mathbf{r}), \check{\tau}_{\ell\ell'}^{\downarrow}(\mathbf{r}')) \sim e^{-\lambda(\tau_{\ell'-1}(y) - \tau_{\ell'}(y'))}$$

vanishes exponentially as $\lambda \rightarrow +\infty$.

The cases in which the target and the source are located in different layers are illustrated by Fig. 3.2 for $\ell < \ell'$, and Fig. 3.3 for $\ell > \ell'$, respectively. The only difference with the previous case is that one of the reaction field components has minimal vertical transmission distance given by $|y - y'|$. This component must exist because it is *not* equivalent to the free-space interaction due to the transmission through multiple layers.

In later discussion of the FMM implementation, the “effective” field transmission distance

$$d_{\ell\ell'}^{**}(\mathbf{r}, \mathbf{r}') = |\hat{\tau}_{\ell\ell'}^{**}(\mathbf{r}) - \check{\tau}_{\ell\ell'}^{**}(\mathbf{r}')| \quad (3.21)$$

will be used as the criterion of far-field expansions. Note that the field transmission distance is not shorter than that based on equivalent polarization source alone in our previous works [25, 34], suggesting that wave sources in layered media are even more separated than previously thought.

3.3. Indirect boundary integral equation and Nyström method

By using the layered Green's function $G_{\ell\ell'}(\mathbf{r}, \mathbf{r}')$ presented above, the solution of (2.11) has boundary integral representation

$$u^s(\mathbf{r}') = \sum_{\ell=0}^L \frac{\eta_\ell}{\eta_{\ell'}} \int_{\Gamma_\ell} \phi(\mathbf{r}) G_{\ell\ell'}(\mathbf{r}, \mathbf{r}') \, ds, \quad \mathbf{r}' \in \Upsilon_{\ell'} \setminus \Omega_{\ell'}. \quad (3.22)$$

It is worthy to point out that the integral is only on the boundaries of the scatterers, due to the usage of the layered Green's function. Applying boundary condition on $\{\Gamma_\ell\}_{\ell=0}^L$ gives integral equations

$$\sum_{\ell=0}^L \eta_\ell \int_{\Gamma_\ell} \phi(\mathbf{r}) G_{\ell\ell'}(\mathbf{r}, \mathbf{r}') \, ds = \eta_{\ell'} g(\mathbf{r}'), \quad \mathbf{r}' \in \Gamma_{\ell'}, \ell' = 0, 1, \dots, L. \quad (3.23)$$

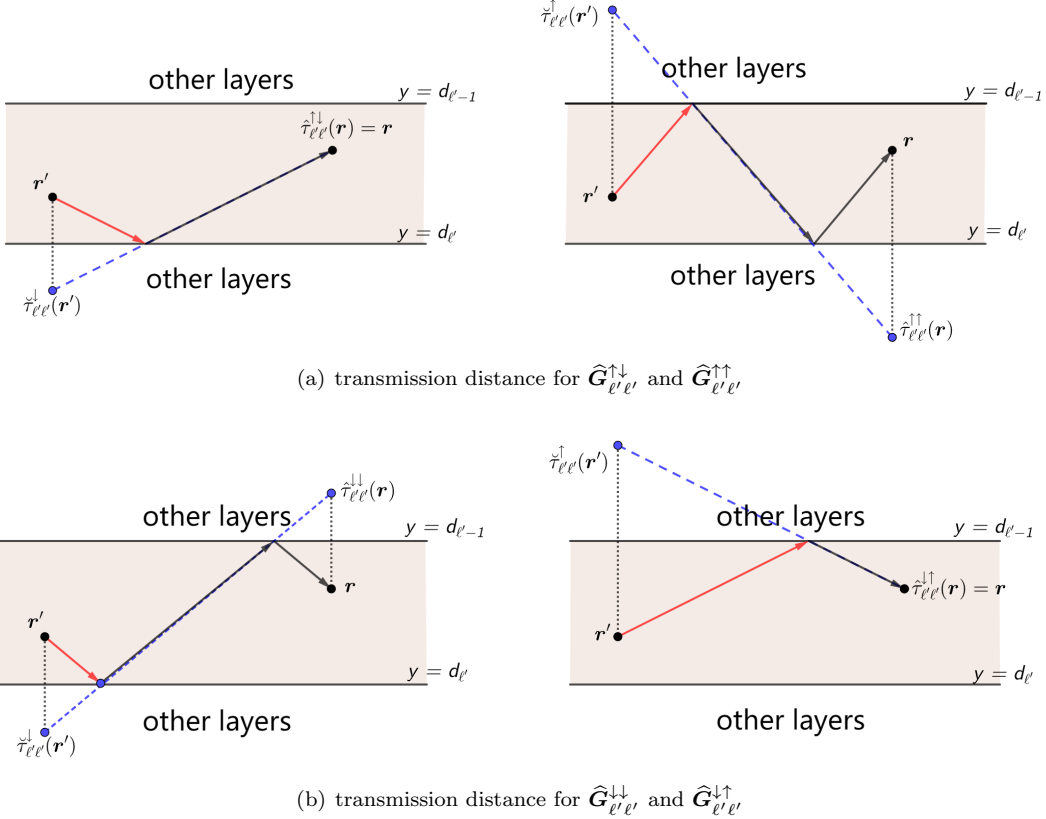


Figure 3.1: Equivalent polarization source coordinates and effective target locations in the case of $\ell = \ell'$.

For the discretization of the integral equations in (3.23), all boundaries $\{\Gamma_\ell\}_{\ell=0}^L$ are discretized into line segments as

$$\Gamma_\ell \approx \bigcup_{e=1}^{N_\ell} \Gamma_{\ell e}, \quad \ell = 0, 1, \dots, L,$$

where N_ℓ denotes the number of elements in the mesh of Γ_ℓ . The total number of elements is denoted by $N = \sum_{\ell=0}^L N_\ell$. On each line element $\Gamma_{\ell e}$, we approximate the density function $\phi(\mathbf{r})$ by a constant function $\phi_{\ell e}$. Substituting into (3.23) and approximating the boundaries by $\{\Gamma_{\ell e}\}_{e=1}^{N_\ell}, \ell = 0, 1, \dots, L$, we obtain the linear system

$$\sum_{\ell=0}^L \eta_\ell \sum_{e=1}^{N_\ell} \left(\int_{\Gamma_{\ell e}} G_{\ell\ell'}(\mathbf{r}, \mathbf{c}_{\ell'i}) \, ds \right) \phi_{\ell e} = \eta_{\ell'} g(\mathbf{c}_{\ell'i}), \quad \mathbf{c}_{\ell'i} \in \Gamma_{\ell'i}, \quad (3.24)$$

for $i = 1, 2, \dots, N_{\ell'}, \ell' = 0, 1, \dots, L$, where the collocation point $\mathbf{c}_{\ell'i}$ is set to be the center of the element $\Gamma_{\ell'i}$. It can be written as matrix formulation

$$\mathbb{K}\Phi = \mathbf{b}, \quad (3.25)$$

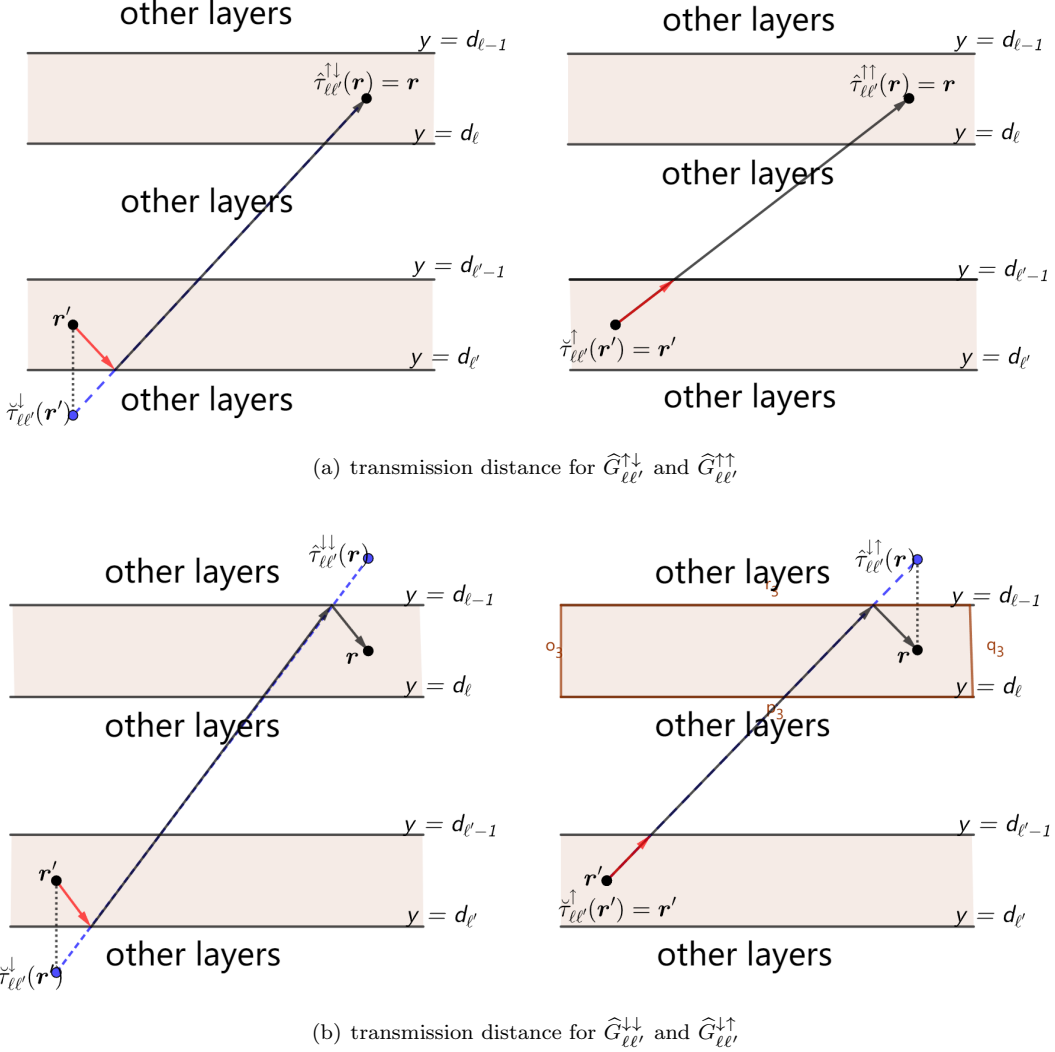


Figure 3.2: Equivalent polarization source coordinates and effective target locations in the case of $\ell < \ell'$.

where

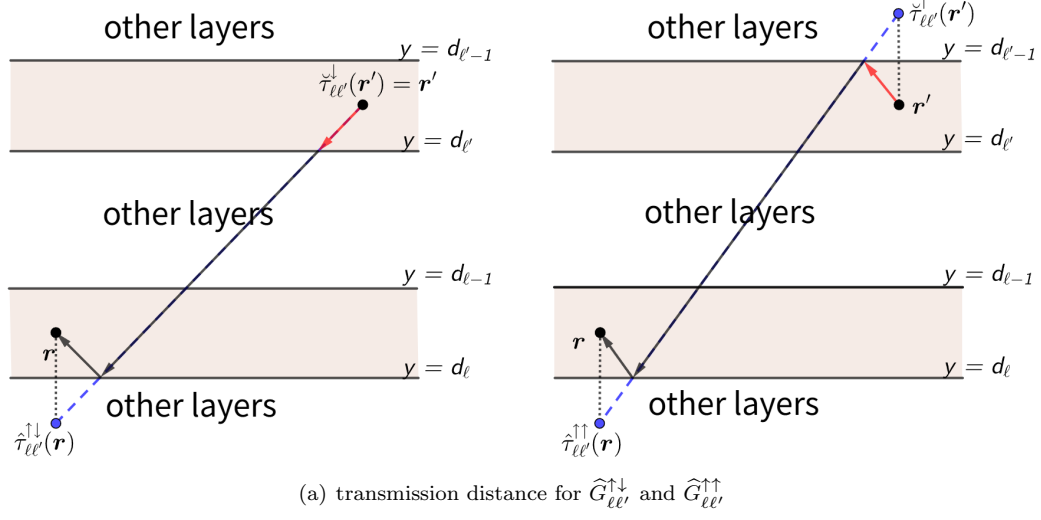
$$\mathbb{K} = \begin{bmatrix} \mathbb{K}_{00} & \mathbb{K}_{01} & \cdots & \mathbb{K}_{0L} \\ \mathbb{K}_{10} & \mathbb{K}_{11} & \cdots & \mathbb{K}_{1L} \\ \vdots & \vdots & \ddots & \vdots \\ \mathbb{K}_{L0} & \mathbb{K}_{L1} & \cdots & \mathbb{K}_{LL} \end{bmatrix}, \quad \Phi = \begin{bmatrix} \Phi_0 \\ \Phi_1 \\ \vdots \\ \Phi_L \end{bmatrix}, \quad \mathbf{b} = \begin{bmatrix} \mathbf{b}_0 \\ \mathbf{b}_1 \\ \vdots \\ \mathbf{b}_L \end{bmatrix}, \quad (3.26)$$

with dense blocks

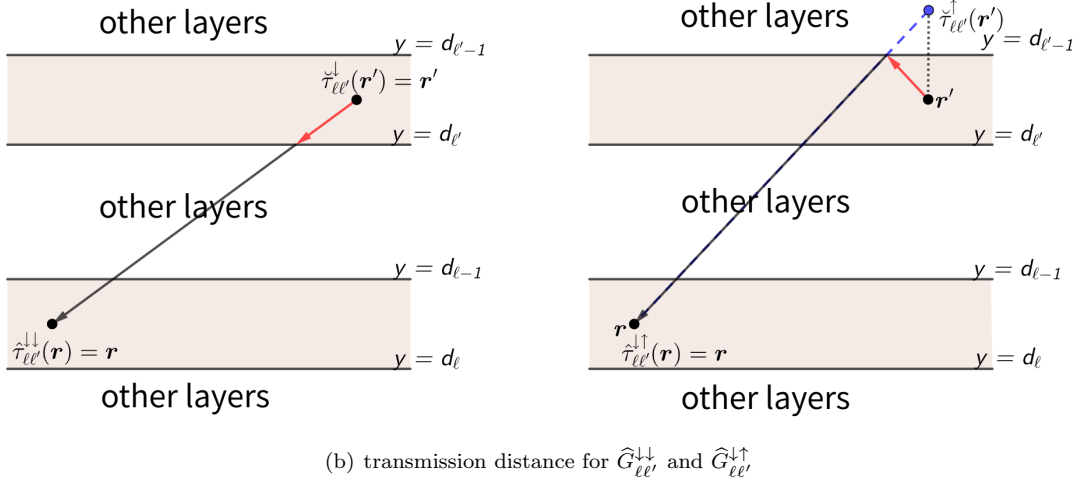
$$\mathbb{K}_{\ell\ell'} = (K_{ei}^{\ell\ell'})_{N_{\ell'} \times N_{\ell}}, \quad K_{ei}^{\ell\ell'} = \int_{\Gamma_{\ell e}} G_{\ell\ell'}(\mathbf{r}, \mathbf{c}_{\ell'} i) \, ds, \quad (3.27)$$

and

$$\Phi_{\ell}^T = [\eta_{\ell}\phi_{\ell 1} \quad \eta_{\ell}\phi_{\ell 2} \quad \cdots \quad \eta_{\ell}\phi_{\ell, N_{\ell}}], \quad \mathbf{b}_{\ell}^T = [\eta_{\ell}g(c_{\ell 1}) \quad \eta_{\ell}g(c_{\ell 2}) \quad \cdots \quad \eta_{\ell}g(c_{\ell, N_{\ell}})],$$



(a) transmission distance for $\hat{G}_{\ell\ell'}^{\downarrow\downarrow}$ and $\hat{G}_{\ell\ell'}^{\uparrow\uparrow}$



(b) transmission distance for $\hat{G}_{\ell\ell'}^{\downarrow\downarrow}$ and $\hat{G}_{\ell\ell'}^{\uparrow\uparrow}$

Figure 3.3: Equivalent polarization source coordinates and effective target locations in the case of $\ell > \ell'$.

for $\ell, \ell' = 0, 1, \dots, L$.

Substituting the layered Green's function (3.8) into the expression (3.27) for $K_{ei}^{\ell\ell'}$, gives

$$K_{ei}^{\ell\ell'} = \delta_{\ell\ell'} \int_{\Gamma_{\ell e}} G_{\ell}^f(\mathbf{r}, \mathbf{c}_{\ell'i}) \, ds + \int_{\Gamma_{\ell e}} G_{\ell\ell'}^r(\mathbf{r}, \mathbf{c}_{\ell'i}) \, ds. \quad (3.28)$$

Let us first consider the computation of the diagonal entries $K_{ii}^{\ell'\ell'}, \ell' = 0, 1, \dots, L; i = 1, 2, \dots, N_{\ell'}$. Note that $G_{\ell'}^f(\mathbf{r}, \mathbf{c}_{\ell'i})$ has weak singularity at $\mathbf{r} = \mathbf{c}_{\ell'i}$ while $G_{\ell\ell'}^r(\mathbf{r}, \mathbf{c}_{\ell'i})$ is smooth in the element $\Gamma_{\ell'i}$. Therefore, the second term in the equation (3.28) can be directly approximated by

$$\int_{\Gamma_{\ell'i}} G_{\ell'\ell'}^r(\mathbf{r}, \mathbf{c}_{\ell'i}) \, ds \approx G_{\ell'\ell'}^r(\mathbf{c}_{\ell'i}, \mathbf{c}_{\ell'i}) |\Gamma_{\ell'i}|. \quad (3.29)$$

For weakly singular term, utilizing the asymptotic behavior

$$H_0^{(1)}(z) \sim 1 + \frac{2i}{\pi} \left(\ln \frac{z}{2} + \gamma \right), \quad z \rightarrow 0,$$

where γ denotes the Euler constant, we decompose the integral into weakly singular and regular terms as follows

$$\begin{aligned} \int_{\Gamma_{\ell'i}} G_{\ell'}^f(\mathbf{r}, \mathbf{c}_{\ell'i}) \, ds &= \frac{i}{4} \int_{\Gamma_{\ell'i}} \left[H_0^{(1)}(k_{\ell'}|\mathbf{r} - \mathbf{c}_{\ell'i}|) - 1 - \frac{2i}{\pi} \left(\ln \frac{k_{\ell'}|\mathbf{r} - \mathbf{c}_{\ell'i}|}{2} + \gamma \right) \right] \, ds \\ &\quad + \frac{i}{4} \int_{\Gamma_{\ell'i}} \left[1 + \frac{2i}{\pi} \left(\ln \frac{k_{\ell'}|\mathbf{r} - \mathbf{c}_{\ell'i}|}{2} + \gamma \right) \right] \, ds \\ &:= I_{\ell'i}^r(\mathbf{r}) + I_{\ell'i}^s(\mathbf{r}). \end{aligned}$$

For the regular term $I_{\ell'i}^r(\mathbf{r})$, the rectangle method yields approximation $I_{\ell'i}^r(\mathbf{c}_{\ell e}) \approx 0$. For the weakly singular term $I_{\ell'i}^s(\mathbf{r})$, it is analytically tractable through integration by parts, i.e.,

$$I_{\ell'i}^s(\mathbf{c}_{\ell'i}) = \left[\frac{i}{4} - \frac{1}{2\pi} \left(\gamma + \ln \frac{k_{\ell'}|\Gamma_{\ell'i}|}{4} - 1 \right) \right] |\Gamma_{\ell'i}|. \quad (3.30)$$

For all off-diagonal entries, i.e., $(\ell, e) \neq (\ell', i)$, the integrand is regular in the integral domain and we are able to use the rectangle method for approximation. In summary, we shall use approximations

$$K_{ei}^{\ell\ell'} \approx \begin{cases} G_{\ell'\ell'}^r(\mathbf{c}_{\ell'i}, \mathbf{c}_{\ell'i}) |\Gamma_{\ell'i}| + I_{\ell'i}^s(\mathbf{c}_{\ell'i}), & (\ell, e) = (\ell', i), \\ G_{\ell\ell'}(\mathbf{c}_{\ell e}, \mathbf{c}_{\ell'i}) |\Gamma_{\ell e}|, & (\ell, e) \neq (\ell', i). \end{cases} \quad (3.31)$$

According to (3.26), (3.27) and (3.31), the coefficient matrix \mathbb{K} is a non-symmetric dense matrix. Consequently, the linear system (3.25) can be solved by direct methods such as LU factorization or Gaussian elimination, though these require $\mathcal{O}(N^3)$ operations. Alternatively, Krylov subspace iterative methods including GMRES, BiCG, could be employed. Therefore, the core computational task involves computing the matrix-vector product $\Phi^{(k+1)} = \mathbb{K}\Phi^{(k)}$ at each iteration k , where the iterate vector is defined as

$$\Phi^{(k)} = \begin{bmatrix} \Phi_0^{(k)} & \Phi_1^{(k)} & \dots & \Phi_L^{(k)} \end{bmatrix}^T.$$

Denoted the resultant vector by $\Phi^{(k+1)} = (\Phi_{\ell'i}^{(k+1)})_{N \times 1}$, each component $\Phi_{\ell'i}^{(k+1)}$ is computed as follows

$$\Phi_{\ell'i}^{(k+1)} \approx \sum_{\ell=0}^L \sum_{e=1}^{N_\ell} G_{\ell\ell'}^r(\mathbf{c}_{\ell e}, \mathbf{c}_{\ell'i}) Q_{\ell e} + \sum_{\substack{e=1 \\ e \neq i}}^{N_{\ell'}} G_{\ell'}^f(\mathbf{c}_{\ell e}, \mathbf{c}_{\ell'i}) Q_{\ell e} + I_{\ell'i}^s(\mathbf{c}_{\ell'i}) \eta_{\ell'} \phi_{\ell'i}^{(k)}, \quad (3.32)$$

where $Q_{\ell e} = \eta_{\ell} \phi_{\ell e}^{(k)} |\Gamma_{\ell e}|$. Here, the approximations (3.31) and ((3.30)) for $K_{ie}^{\ell\ell'}$ have been used. Define

$$\Phi_{\ell'i}^f = \sum_{\substack{e=1 \\ e \neq i}}^{N_{\ell'}} G_{\ell'}^f(\mathbf{c}_{\ell e}, \mathbf{c}_{\ell'i}) Q_{\ell e}, \quad \Phi_{\ell'i}^r = \sum_{\ell=0}^L \sum_{e=1}^{N_\ell} Q_{\ell e} G_{\ell\ell'}^r(\mathbf{c}_{\ell e}, \mathbf{c}_{\ell'i}). \quad (3.33)$$

Then, the matrix product vector (3.32) can be re-expressed as

$$\Phi_{\ell'i}^{(k+1)} = \Phi_{\ell'i}^f + \Phi_{\ell'i}^r + I_{\ell'i}^s(\mathbf{c}_{\ell'i}) \eta_{\ell'} \phi_{\ell'i}^{(k+1)}, \quad i = 1, 2, \dots, N_{\ell'}; \ell' = 0, 1, \dots, L. \quad (3.34)$$

Direct computation incurs $\mathcal{O}(N^2)$ cost for each iteration. Therefore, both direct and iterative methods become computationally infeasible for large-scale problems.

4. Fast multipole acceleration and preconditioning

In this section, we have improved a fast multipole method (FMM) from our previous work (cf.[34, 25]), which accelerates matrix-vector products $\Phi^{(k+1)} = \mathbb{K}\Phi^{(k)}$ within the iterative solver. This technique reduces the computational cost per iteration to $\mathcal{O}(N \log N)$.

The formulation (3.34) shows that $\{\Phi_{\ell' i}^f\}_{i=1}^{N_{\ell'}}$ and $\{\Phi_{\ell' i}^r\}_{i=1}^{N_{\ell'}}$ can be computed separately. For free-space parts $\{\Phi_{\ell' i}^f\}_{i=1}^{N_{\ell'}}$, the classical FMM can reduce the cost to $\mathcal{O}(N_{\ell'} \log N_{\ell'})$ per layer. The main challenge therefore lies in accelerating the computation of the reaction field components $\{\Phi_{\ell' i}^r\}_{i=1}^{N_{\ell'}}$.

From the reaction kernel $G_{\ell\ell'}^r(\mathbf{r}, \mathbf{r}')$ in (3.10)-(3.11), $\Phi_{\ell' i}^r$ admits the decomposition

$$\Phi_{\ell' i}^r = \sum_{\ell=0}^L [\Phi_{\ell\ell'}^{\uparrow\downarrow}(\mathbf{r}_{\ell' i}) + \Phi_{\ell\ell'}^{\uparrow\uparrow}(\mathbf{r}_{\ell' i}) + \Phi_{\ell\ell'}^{\downarrow\uparrow}(\mathbf{r}_{\ell' i}) + \Phi_{\ell\ell'}^{\downarrow\downarrow}(\mathbf{r}_{\ell' i})], \quad (4.1)$$

where

$$\Phi_{\ell\ell'}^{**}(\mathbf{r}_{\ell' i}) = \sum_{e=1}^{N_{\ell}} Q_{\ell e} G_{\ell\ell'}^{**}(\mathbf{r}_{\ell e}, \mathbf{r}_{\ell' i}) = \sum_{e=1}^{N_{\ell}} \frac{Q_{\ell e}}{2\pi} \int_{-\infty}^{\infty} \frac{\mathcal{E}_{\ell\ell'}(\lambda, \hat{\tau}_{\ell\ell'}^{**}(\mathbf{r}_{\ell e}), \check{\tau}_{\ell\ell'}^{*}(\mathbf{r}_{\ell' i}))}{2k_{\ell e, y}} \sigma_{\ell\ell'}^{**}(\lambda) d\lambda, \quad (4.2)$$

for $*, \star = \uparrow, \downarrow$. This is a uniform integral representation for any reaction components indicated by quadruple $(\ell, \ell', *, \star)$. Hence, we generally need to compute the following summations

$$\begin{aligned} \Phi^+(\mathbf{r}_i, \sigma) &= \sum_{j=1}^{M_s} Q'_j \mathcal{I}_{00}^{k'k}(x'_j - x_i, y'_j, y_i, \sigma), \quad i = 1, \dots, M_t, \\ \Phi^-(\mathbf{r}_i, \sigma) &= \sum_{j=1}^{M_s} Q''_j \mathcal{I}_{00}^{kk''}(x''_j - x_i, y_i, y''_j, \sigma), \quad i = 1, \dots, M_t, \end{aligned} \quad (4.3)$$

where the target points $\{\mathbf{r}_i = (x_i, y_i)\}_{i=1}^{M_t}$ and the source points $\{\mathbf{r}'_j = (x'_j, y'_j)\}_{j=1}^{M_s}$ or $\{\mathbf{r}''_j = (x''_j, y''_j)\}_{j=1}^{M_s}$ should be obtained by the reflections $\hat{\tau}_{\ell\ell'}^{**}$, $\check{\tau}_{\ell\ell'}^{*}$ of the original target and source points $\mathbf{r}_{\ell e}, \mathbf{r}_{\ell' i}$ accordingly, k, k' and σ is the triple $(k_{\ell}, k_{\ell'}, \sigma_{\ell\ell'}^{**})$ determined according to quadruple $(\ell, \ell', *, \star)$ and $\mathcal{I}_{00}^{kk'}(x, y, y', \sigma)$ is defined in (4.7). Due to the reflections, we always have the source and target points are separate by one of the interface in the computation of $\Phi^{\pm}(\mathbf{r}_i, \sigma)$. Moreover, the reflection always ensure that $y'_j > y_i$ and $y_i > y''_j$.

4.1. Fast multipole method for reaction components

The basic theory for the FMM of two-dimensional Helmholtz equation in layered media is reported in [34], but without using the concept of effective locations for the target points. In this subsection, we apply this theory to the potentials (4.3) which are defined using both effective locations for targets and equivalent polarization coordinates for sources and provide details for the implementation of the FMM.

The key ingredients in the derivation of the expansion theory are the following expansions obtained by the formulation of the generating function of the cylindrical Bessel functions of the first kind. We refer to [34] for detailed derivation.

Proposition 4.1. *Given four points $\mathbf{r} = (x, y), \mathbf{r}' = (x', y')$, $\mathbf{r}_c = (x_c, y_c)$ and $\mathbf{r}'_c = (x'_c, y'_c)$ in \mathbb{R}^2 such that $|\mathbf{r} - \mathbf{r}_c| < |\mathbf{r}' - \mathbf{r}_c|$ and $|\mathbf{r} - \mathbf{r}'_c| > |\mathbf{r}' - \mathbf{r}'_c|$. Suppose $y > y'$, $y > y'_c$ and $y_c > y'$. Denoted by*

$$\mathcal{E}^{kk'}(x, y, y') = e^{i\lambda x + i\sqrt{k^2 - \lambda^2}y - i\sqrt{k'^2 - \lambda^2}y'}, \quad (4.4)$$

then there holds the following expansions

$$\begin{aligned}\mathcal{E}^{kk'}(x - x', y, y') &= \sum_{n=-\infty}^{\infty} J_n(k\rho_c) e^{in\theta_c} \omega(\lambda, k)^n \mathcal{E}^{kk'}(x_c - x', y_c, y'), \\ \mathcal{E}^{kk'}(x - x', y, y') &= \sum_{n=-\infty}^{\infty} (-1)^n J_n(k'\rho'_c) e^{in\theta'_c} \omega(\lambda, k')^n \mathcal{E}^{kk'}(x - x'_c, y, y'_c),\end{aligned}\quad (4.5)$$

where

$$w(\lambda, k) = \frac{\sqrt{k^2 - \lambda^2} + i\lambda}{k}, \quad (4.6)$$

(ρ'_c, θ'_c) and (ρ_c, θ_c) are the polar coordinates of $\mathbf{r}' - \mathbf{r}'_c$ and $\mathbf{r} - \mathbf{r}_c$, respectively.

Define

$$\mathcal{I}_{nm}^{kk'}(x, y, y', \sigma) := \int_{-\infty}^{\infty} \mathcal{E}^{kk'}(x, y, y') \omega(\lambda, k)^n \omega(\lambda, k')^m \sigma(\lambda) d\lambda \quad n, m \in \mathbb{Z}. \quad (4.7)$$

Then using the expansions (4.5) inside the integral and then exchange the order of the infinite summation and integral, we obtain

$$\mathcal{I}_{0m}^{kk'}(x - x', y, y', \sigma) = \sum_{n=-\infty}^{\infty} J_n(k\rho_c) e^{in\theta_c} \mathcal{I}_{nm}^{kk'}(x_c - x', y_c, y', \sigma), \quad m = 0, 1, \dots, \quad (4.8)$$

and

$$\mathcal{I}_{m0}^{kk'}(x - x', y, y', \sigma) = \sum_{n=-\infty}^{\infty} (-1)^n J_n(k'\rho'_c) e^{in\theta'_c} \mathcal{I}_{mn}^{kk'}(x - x'_c, y, y'_c, \sigma), \quad m = 0, 1, \dots, \quad (4.9)$$

respectively. The convergence of the above expansions has been proved and verified in [34].

Given source center (x'_c, y'_c) , (x''_c, y''_c) close to the source points, the expansion (4.8) and (4.9) gives

$$\begin{aligned}\mathcal{I}_{00}^{k'k}(x'_j - x_i, y'_j, y_i, \sigma) &= \sum_{n=-\infty}^{\infty} J_n(k'\rho'_j) e^{in\theta'_j} \mathcal{I}_{n0}^{k'k}(x'_c - x_i, y'_c, y_i, \sigma), \\ \mathcal{I}_{00}^{kk''}(x''_j - x_i, y_i, y''_j, \sigma) &= \sum_{n=-\infty}^{\infty} (-1)^n J_n(k''\rho''_j) e^{in(\pi - \theta''_j)} \mathcal{I}_{0n}^{kk''}(x''_c - x_i, y_i, y''_c, \sigma), \\ &= \sum_{n=-\infty}^{\infty} J_n(k''\rho''_j) e^{-in\theta''_j} \mathcal{I}_{0n}^{kk''}(x''_c - x_i, y_i, y''_c, \sigma),\end{aligned}\quad (4.10)$$

where (ρ'_j, θ'_j) and (ρ''_j, θ''_j) are the polar coordinates of $(x'_j - x'_c, y'_j - y'_c)$ and $(x''_j - x''_c, y''_j - y''_c)$, respectively. For the derivation of the second expansion, we actually use (4.9) with $(x, y) = (-x_i, y_i)$, $(x', y') = (-x''_j, y''_j)$ and $(x'_c, y'_c) = (-x''_c, y''_c)$.

Therefore, we obtain multipole expansions (ME):

$$\begin{aligned}\Phi^+(\mathbf{r}_i, \sigma) &= \sum_{|n|=0}^{\infty} \alpha_n^+ \mathcal{I}_{n0}^{k'k}(x'_c - x_i, y'_c, y_i, \sigma), \\ \Phi^-(\mathbf{r}_i, \sigma) &= \sum_{|n|=0}^{\infty} \alpha_n^- \mathcal{I}_{0-n}^{kk''}(x''_c - x_i, y_i, y''_c, \sigma),\end{aligned}\quad (4.11)$$

where

$$\alpha_n^+ = \sum_{j=1}^{M_s} Q'_j J_n(k' \rho'_j) e^{in\theta'_j}, \quad \alpha_n^- = \sum_{j=1}^{M_s} (-1)^n Q''_j J_n(k'' \rho''_j) e^{in\theta''_j}. \quad (4.12)$$

Similarly, given the target center (x_c, y_c) close to the target points $\{(x_i, y_i)\}$, the expansion (4.8) and (4.9) gives the local expansions (LE):

$$\Phi^+(\mathbf{r}_i, \sigma) = \sum_{|n|=0}^{\infty} \beta_n^+ J_n(k\rho_i) e^{in\theta_i}, \quad \Phi^-(\mathbf{r}_i, \sigma) = \sum_{|n|=0}^{\infty} \beta_n^- J_n(k\rho_i) e^{in\theta_i}, \quad (4.13)$$

where (ρ_i, θ_i) is the polar coordinates of $(x_i - x_c, y_i - y_c)$, and

$$\beta_n^+ = \sum_{j=1}^{M_s} Q'_j (-1)^n \mathcal{I}_{0n}^{k'k}(x'_j - x_c, y'_j, y_c, \sigma), \quad \beta_n^- = \sum_{j=1}^{M_s} Q''_j \mathcal{I}_{-n0}^{kk''}(x''_j - x_c, y_c, y''_j, \sigma). \quad (4.14)$$

Let $(\tilde{x}'_c, \tilde{y}'_c)$ be another source center close to (x'_c, y'_c) and $(\tilde{x}''_c, \tilde{y}''_c)$ be another source center close to (x''_c, y''_c) . Then, the multipole expansions with respect to new source centers $(\tilde{x}'_c, \tilde{y}'_c)$ and $(\tilde{x}''_c, \tilde{y}''_c)$ are given by

$$\begin{aligned} \Phi^+(\mathbf{r}_i, \sigma) &= \sum_{|n|=0}^{\infty} \tilde{\alpha}_n^+ \mathcal{I}_{n0}^{kk'}(\tilde{x}'_c - x_i, \tilde{y}'_c, y_i, \sigma), \\ \Phi^-(\mathbf{r}_i, \sigma) &= \sum_{|n|=0}^{\infty} \tilde{\alpha}_n^- \mathcal{I}_{0,-n}^{kk''}(\tilde{x}''_c - x_i, y_i, \tilde{y}''_c, \sigma), \end{aligned} \quad (4.15)$$

where

$$\tilde{\alpha}_n^+ = \sum_{j=1}^{M_s} Q'_j J_n(k' \tilde{\rho}'_j) e^{in\tilde{\theta}'_j}, \quad \tilde{\alpha}_n^- = \sum_{j=1}^{M_s} (-1)^n Q''_j J_n(k'' \tilde{\rho}''_j) e^{in\tilde{\theta}''_j}, \quad (4.16)$$

$(\tilde{\rho}'_j, \tilde{\theta}'_j)$ and $(\tilde{\rho}''_j, \tilde{\theta}''_j)$ are the polar coordinates of $(x'_j - \tilde{x}'_c, y'_j - \tilde{y}'_c)$ and $(x''_j - \tilde{x}''_c, y''_j - \tilde{y}''_c)$. By Graf's addition theorem (cf. [40]), we have M2M shifting operators:

$$\tilde{\alpha}_n^+ = \sum_{|m|=0}^{\infty} J_{n-m}(k\rho'_c) e^{i(n-m)\theta'_c} \alpha_m^+, \quad \tilde{\alpha}_n^- = \sum_{|m|=0}^{\infty} J_{m-n}(k''\rho''_c) e^{i(n-m)\theta''_c} \alpha_m^-, \quad (4.17)$$

where (ρ'_c, θ'_c) and (ρ''_c, θ''_c) are the polar coordinates of $(x'_c - \tilde{x}'_c, y_c - \tilde{y}'_c)$ and $(x''_c - \tilde{x}''_c, y_c - \tilde{y}''_c)$.

Let $(\tilde{x}_c, \tilde{y}_c)$ be another target center close to (x_c, y_c) . By the local expansions in (4.13) and Graf's addition theorem (cf. [40]), we have

$$\Phi^+(\mathbf{r}_i, \sigma) = \sum_{|n|=0}^{\infty} \tilde{\beta}_n^+ J_n(k\tilde{\rho}_i) e^{in\tilde{\theta}_i}, \quad \Phi^-(\mathbf{r}_i, \sigma) = \sum_{|n|=0}^{\infty} \tilde{\beta}_n^- J_n(k\tilde{\rho}_i) e^{in\tilde{\theta}_i}, \quad (4.18)$$

where

$$\tilde{\beta}_n^+ = \sum_{|m|=0}^{\infty} J_m(k\tilde{\rho}_c) e^{im\tilde{\theta}_c} \beta_{n+m}^+, \quad \tilde{\beta}_n^- = \sum_{|m|=0}^{\infty} (-1)^m J_m(k\tilde{\rho}_c) e^{-im\tilde{\theta}_c} \beta_{m-n}^-, \quad (4.19)$$

are the L2L shifting operators and $(\tilde{\rho}_i, \tilde{\theta}_i)$ and $(\tilde{\rho}_c, \tilde{\theta}_c)$ are the polar coordinates of $(x_i - \tilde{x}_c, y_i - \tilde{y}_c)$ and $(x_c - \tilde{x}_c, y_c - \tilde{y}_c)$.

Next, we consider the multipole-to-local translation. Applying expansion formulations (4.8)-(4.9) to the multipole expansions in (4.10), we obtain

$$\begin{aligned}\psi^+(\mathbf{r}_i, \sigma) &= \sum_{|m|=0}^{\infty} \sum_{|n|=0}^{\infty} \alpha_n^+(-1)^m J_m(k\rho_i) e^{im\theta_i} \mathcal{I}_{nm}^{k'k}(x'_c - x_c, y'_c, y_c, \sigma), \\ \psi^-(\mathbf{r}_i, \sigma) &= \sum_{|m|=0}^{\infty} \sum_{|n|=0}^{\infty} \alpha_n^-(-1)^m J_m(k\rho_i) e^{-im\theta_i} \mathcal{I}_{mn}^{kk''}(x''_c - x_c, y_c, y''_c, \sigma).\end{aligned}$$

Matching with the local expansions in (4.13) gives M2L translations

$$\beta_m^+ = \sum_{|n|=0}^{\infty} (-1)^m \mathcal{I}_{nm}^{k'k}(x'_c - x_c, y'_c, y_c, \sigma) \alpha_n^+, \quad \beta_m^- = \sum_{|n|=0}^{\infty} \mathcal{I}_{-mn}^{kk''}(x''_c - x_c, y_c, y''_c, \sigma) \alpha_n^-. \quad (4.20)$$

Using the truncated expansions, shifting and translation operators in the framework of the classic FMM, we implement a FMM for fast calculation of $\{\Phi^\pm(\mathbf{r}_i, \sigma)\}_{i=1}^{M_t}$ at any desired accuracy. The pseudo-code of the algorithm and the overall FMM for the computation of the interactions defined in (4.2) is similar to the algorithms we have reported in our previous work [25]. Our implementation actually used the adaptive tree structure by changing the FMM framework to its adaptive version (cf. [41]).

4.2. An overlapping domain decomposition preconditioner

Obviously, equation (3.23) is a first-kind Fredholm integral equation. By the compactness of the integral operator and the spectral theory of compact operators, it has an infinite condition number. Although the discretized linear system (3.24) is an approximation of the integral equation (3.23) and thus exhibits a finite condition number, its value grows unbounded as the degree of freedom increases. Such an ill-conditioning severely degrades the convergence rate of iterative solvers. To enable efficient large-scale simulations, we will use a preconditioning technique for capacitance extraction of conductors (cf. [42]) to develop a tailored preconditioning framework for layered media problems. Specifically, high performance can be achieved by applying overlapping domain decomposition preconditioning within each layer.

Recall the approximations in (3.31), each diagonal block of the matrix \mathbb{K} has the form

$$\mathbb{K}_{\ell\ell} = \begin{bmatrix} |\Gamma_{\ell 1}| G_{\ell\ell}^r(\mathbf{c}_{\ell 1}, \mathbf{c}_{\ell 1}) + I_{\ell 1}^s(\mathbf{c}_{\ell 1}) & |\Gamma_{\ell 2}| G_{\ell\ell}^r(\mathbf{c}_{\ell 2}, \mathbf{c}_{\ell 1}) & \cdots & |\Gamma_{\ell N_\ell}| G_{\ell\ell}^r(\mathbf{c}_{\ell N_\ell}, \mathbf{c}_{\ell 1}) \\ |\Gamma_{\ell 1}| G_{\ell\ell}^r(\mathbf{c}_{\ell 1}, \mathbf{c}_{\ell 2}) & |\Gamma_{\ell 2}| G_{\ell\ell}^r(\mathbf{c}_{\ell 2}, \mathbf{c}_{\ell 2}) + I_{\ell 2}^s(\mathbf{c}_{\ell 2}) & \cdots & |\Gamma_{\ell N_\ell}| G_{\ell\ell}^r(\mathbf{c}_{\ell N_\ell}, \mathbf{c}_{\ell 2}) \\ \vdots & \vdots & \ddots & \vdots \\ |\Gamma_{\ell 1}| G_{\ell\ell}^r(\mathbf{c}_{\ell 1}, \mathbf{c}_{\ell N_\ell}) & |\Gamma_{\ell 2}| G_{\ell\ell}^r(\mathbf{c}_{\ell 2}, \mathbf{c}_{\ell N_\ell}) & \cdots & |\Gamma_{\ell N_\ell}| G_{\ell\ell}^r(\mathbf{c}_{\ell N_\ell}, \mathbf{c}_{\ell N_\ell}) + I_{\ell N_\ell}^s(\mathbf{c}_{\ell N_\ell}) \end{bmatrix},$$

for all $\ell = 0, 1, \dots, L$. We ignore the reaction field component $G_{\ell\ell'}^r$ in the diagonal blocks $\mathbb{K}_{\ell\ell}$ and define

$$\tilde{\mathbb{K}}_{\ell\ell} = \begin{bmatrix} I_{\ell 1}^s(\mathbf{c}_{\ell 1}) & |\Gamma_{\ell 2}| G_{\ell}^f(\mathbf{c}_{\ell 2}, \mathbf{c}_{\ell 1}) & \cdots & |\Gamma_{\ell N_\ell}| G_{\ell}^f(\mathbf{c}_{\ell N_\ell}, \mathbf{c}_{\ell 1}) \\ |\Gamma_{\ell 1}| G_{\ell}^f(\mathbf{c}_{\ell 1}, \mathbf{c}_{\ell 2}) & I_{\ell 2}^s(\mathbf{c}_{\ell 2}) & \cdots & |\Gamma_{\ell N_\ell}| G_{\ell}^f(\mathbf{c}_{\ell N_\ell}, \mathbf{c}_{\ell 2}) \\ \vdots & \vdots & \ddots & \vdots \\ |\Gamma_{\ell 1}| G_{\ell}^f(\mathbf{c}_{\ell 1}, \mathbf{c}_{\ell N_\ell}) & |\Gamma_{\ell 2}| G_{\ell}^f(\mathbf{c}_{\ell 2}, \mathbf{c}_{\ell N_\ell}) & \cdots & I_{\ell N_\ell}^s(\mathbf{c}_{\ell N_\ell}) \end{bmatrix},$$

then, we obtain an approximation for diagonal part of \mathbb{K} , i.e.,

$$\tilde{\mathbb{K}} = \begin{bmatrix} \tilde{\mathbb{K}}_{00} & 0 & \cdots & 0 \\ 0 & \tilde{\mathbb{K}}_{11} & \cdots & 0 \\ \vdots & \vdots & \ddots & \vdots \\ 0 & 0 & \cdots & \tilde{\mathbb{K}}_{LL} \end{bmatrix}.$$

Although $\tilde{\mathbb{K}}$ is block-diagonal, each block corresponds to an approximation of a free space scattering problem within a single layer, whose solution remains computationally expensive. To address this, we leverage the tree structure generated by the FMM to construct an approximation of $\tilde{\mathbb{K}}^{-1}$ as a preconditioner for solving the linear system (3.25).

The spatial decay property of the free-space Green's function (3.9) implies that $|G_\ell^f(\mathbf{r}, \mathbf{r}')| \rightarrow 0$ as $|\mathbf{r} - \mathbf{r}'| \rightarrow \infty$. Consequently, matrix entries $|\Gamma_{\ell j}|G_\ell^f(\mathbf{c}_{\ell j}, \mathbf{c}_{\ell k})$ in $\tilde{\mathbb{K}}_{\ell\ell}$ exhibit similar decay. This indicates that for any unknown $\phi_{\ell e}$, only strongly related to its nearby unknowns. Thus, in the construction of a preconditioner, influences from distant DOFs can be neglected, a proximity criterion naturally provided by the FMM tree structure.

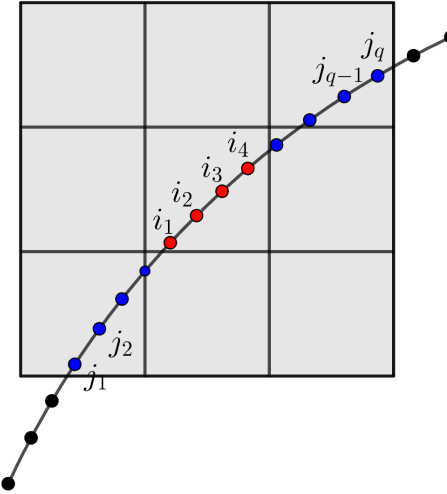


Figure 4.1: Unknowns in the local system for preconditioning.

Within this FMM framework, source and target particles are the same. We now consider any given leaf box $B_{\ell k}$ in the source particle tree corresponding to the FMM for the free space component in the ℓ -th layer. Let $B_{\ell k}$ contain particles associated with DOFs $\phi_{\ell i_1}, \phi_{\ell i_2}, \dots, \phi_{\ell i_p}$, and let its neighbor boxes (including itself) contain DOFs $\phi_{\ell j_1}, \phi_{\ell j_2}, \dots, \phi_{\ell j_q}$, see Fig. 4.1. Apparently, there holds

$$\{i_1, i_2, \dots, i_p\} \subset \{j_1, j_2, \dots, j_q\}.$$

We construct a local linear system

$$\mathbb{P}_{B_{\ell k}} \begin{bmatrix} \tilde{\phi}_{\ell j_1} \\ \tilde{\phi}_{\ell j_2} \\ \vdots \\ \tilde{\phi}_{\ell j_q} \end{bmatrix} = \begin{bmatrix} \eta_{\ell g}(\mathbf{c}_{\ell j_1}) \\ \eta_{\ell g}(\mathbf{c}_{\ell j_2}) \\ \vdots \\ \eta_{\ell g}(\mathbf{c}_{\ell j_q}) \end{bmatrix},$$

where

$$\mathbb{P}_{B_{\ell k}} = \begin{bmatrix} I_{\ell j_1}^s(\mathbf{c}_{\ell j_1}) & |\Gamma_{\ell j_2}|G_\ell^f(\mathbf{c}_{\ell j_2}, \mathbf{c}_{\ell j_1}) & \cdots & |\Gamma_{\ell j_q}|G_\ell^f(\mathbf{c}_{\ell j_q}, \mathbf{c}_{\ell j_1}) \\ |\Gamma_{\ell j_1}|G_\ell^f(\mathbf{c}_{\ell j_1}, \mathbf{c}_{\ell j_2}) & I_{\ell j_2}^s(\mathbf{c}_{\ell j_2}) & \cdots & |\Gamma_{\ell j_q}|G_\ell^f(\mathbf{c}_{\ell j_q}, \mathbf{c}_{\ell j_2}) \\ \vdots & \vdots & \ddots & \vdots \\ |\Gamma_{\ell j_1}|G_\ell^f(\mathbf{c}_{\ell j_1}, \mathbf{c}_{\ell j_q}) & |\Gamma_{\ell j_2}|G_\ell^f(\mathbf{c}_{\ell j_2}, \mathbf{c}_{\ell j_q}) & \cdots & I_{\ell j_q}^s(\mathbf{c}_{\ell j_q}) \end{bmatrix}. \quad (4.21)$$

Then, the components $\tilde{\phi}_{\ell i_1}, \tilde{\phi}_{\ell i_2}, \dots, \tilde{\phi}_{\ell i_p}$ corresponding to the particles within $B_{\ell k}$ are extracted from the solution as an approximation to the original unknowns $\phi_{\ell i_1}, \phi_{\ell i_2}, \dots, \phi_{\ell i_p}$. The inverse operator associated with the superposition of these local solution procedures is denoted by $\mathbb{P}_{\ell\ell}^{-1}$, satisfying:

$$\begin{bmatrix} \tilde{\phi}_{\ell 1} \\ \tilde{\phi}_{\ell 2} \\ \vdots \\ \tilde{\phi}_{\ell N_{\ell}} \end{bmatrix} = \mathbb{P}_{\ell\ell}^{-1} \begin{bmatrix} \eta_{\ell} g(\mathbf{c}_{\ell 1}) \\ \eta_{\ell} g(\mathbf{c}_{\ell 2}) \\ \vdots \\ \eta_{\ell} g(\mathbf{c}_{\ell N_{\ell}}) \end{bmatrix}.$$

Suppose the FMM tree structure for the ℓ -th layer has m_{ℓ} leaf boxes, then

$$\mathbb{P}_{\ell\ell}^{-1} = \sum_{k=1}^{m_{\ell}} \mathbb{S}_{B_{\ell k}} \mathbb{Q}_{B_{\ell k}} \mathbb{P}_{B_{\ell k}}^{-1} \mathbb{R}_{B_{\ell k}},$$

where $\mathbb{R}_{B_{\ell k}}$, $\mathbb{Q}_{B_{\ell k}}$ and $\mathbb{S}_{B_{\ell k}}$ are gather and scatter matrices corresponding to box $B_{\ell k}$ such that

$$\begin{bmatrix} \phi_{\ell j_1} \\ \phi_{\ell j_2} \\ \vdots \\ \phi_{\ell j_q} \end{bmatrix} = \mathbb{R}_{B_{\ell k}} \Phi_{\ell}, \quad \begin{bmatrix} \phi_{\ell i_1} \\ \phi_{\ell i_2} \\ \vdots \\ \phi_{\ell i_p} \end{bmatrix} = \mathbb{Q}_{B_{\ell k}} \begin{bmatrix} \phi_{\ell j_1} \\ \phi_{\ell j_2} \\ \vdots \\ \phi_{\ell j_q} \end{bmatrix}, \quad \Phi_{\ell} = \sum_{k=1}^{m_{\ell}} \mathbb{S}_{B_{\ell k}} \begin{bmatrix} \phi_{\ell i_1} \\ \phi_{\ell i_2} \\ \vdots \\ \phi_{\ell i_p} \end{bmatrix}.$$

Consequently,

$$\mathbb{P}^{-1} = \begin{bmatrix} \mathbb{P}_{00}^{-1} & 0 & \cdots & 0 \\ 0 & \mathbb{P}_{11}^{-1} & \cdots & 0 \\ \vdots & \vdots & \ddots & \vdots \\ 0 & 0 & \cdots & \mathbb{P}_{LL}^{-1} \end{bmatrix}$$

completes the construction of a high-performance preconditioner for the original matrix \mathbb{K} . The effectiveness of the proposed preconditioner will be validated by numerical examples presented in the next section.

5. Numerical Examples

In this section, we present some numerical examples to validate the accuracy and efficiency of the proposed fast boundary integral method to solve multiple scattering problems in layered media. All examples are solved using the lowest order Nyström discretization and FMM accelerated GMRES algorithm with a relative error tolerance of $1.0e-8$.

Example 1. We first test the accuracy of the proposed fast algorithm to solve the scattering problem (2.11) with an exact solution given by

$$u^s(\mathbf{r}) = G_{\ell 0}(\mathbf{r}, \mathbf{r}'), \quad \forall \mathbf{r} \in \Upsilon_{\ell} \setminus \Omega, \quad \ell = 0, 1, 2, 3, 4, \quad (5.1)$$

where Ω is a L-shaped domain with vertices $(0.75, 0.75)$, $(-0.75, 0.75)$, $(-0.75, -2.5)$, $(2.25, -2.5)$, $(2.25, -1.5)$, and $(0.75, -1.5)$, as shown in Fig. 5.1(a), the interfaces of the layered medium are located at $y = \{0, -1, -2, -3\}$. Apparently, the scatterer Ω is embedded in 4 layers. The reflection indices and the wave numbers of the layered media are specified as $\eta = \{1, 2, 3, 4, 5\}$ and $k = \{3.2, 2.5, 5.1, 8.6, 6.9\}$. The exact solution $G_{\ell 0}$ is the Green's function of the layered media with a point source at $\mathbf{r}' = (0, 0.375)$ located inside the L-shaped domain in the 0-th layer.

The performance of the proposed fast algorithm is summarized in Table 5.1. It shows that first-order convergence rates are achieved in both the L_∞ and L_2 norms. By using the preconditioning, the number of iterations decreases significantly, especially when the degree of freedom is large. The numbers of iterations in the GMRES with/without preconditioning are compared in Table 5.1 and Fig. 5.2. Besides, the CPU time of the FMM accelerated iteration and the preconditioning in each step are plotted in Fig. 5.3. Both show $\mathcal{O}(N)$ computational complexity.

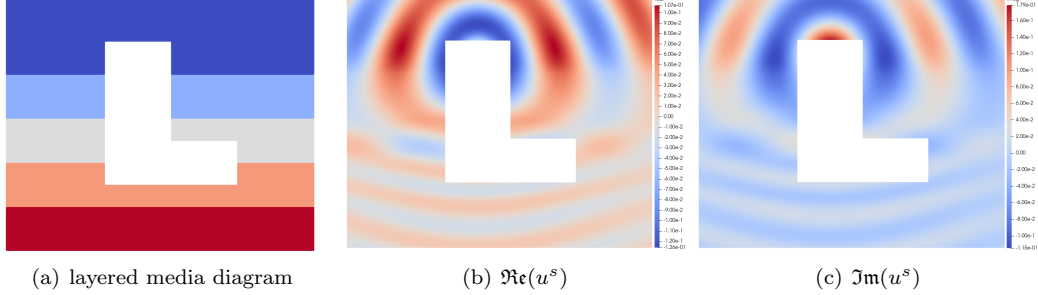


Figure 5.1: Problem diagram and numerical solution

Table 5.1: The performance of the fast algorithm

Elements	Iteration Steps	Iteration Steps with preconditioning	Time(sec)	Time(sec) with preconditioning	L_∞ Error	L_2 Error
12000	140	60	739.71	573.37	2.282e-02	3.064e-04
24000	163	68	918.03	650.14	1.151e-02	1.544e-05
48000	190	77	1142.87	783.46	5.782e-03	7.748e-05
96000	278	86	2110.27	1014.66	2.897e-03	3.884e-05
192000	331	99	3535.53	1501.94	1.450e-03	1.948e-05

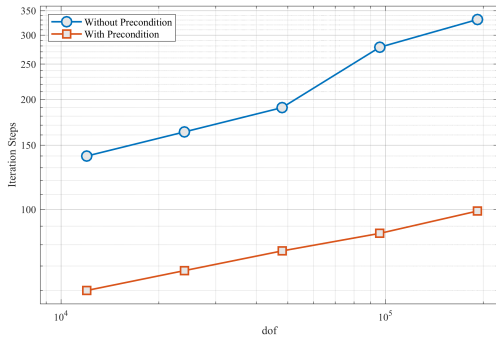


Figure 5.2: Iteration steps vs dof

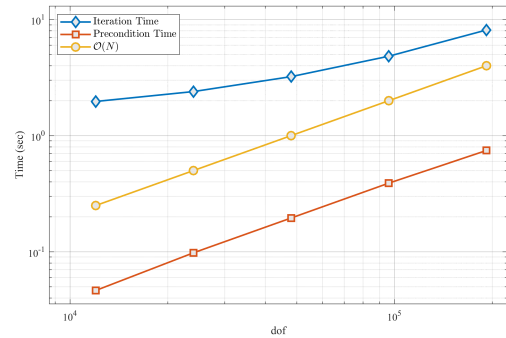


Figure 5.3: Time per iteration step vs dof

Example 2. Consider a layered medium of six layers with interfaces at $y = \{0, -1, -2, -3, -4\}$, where the reflection indices and wave numbers are specified as $\eta = \{1.1, 2.3, 3.4, 4.6, 5.0, 6.6\}$ and $k = \{1.2, 2.3, 4.5, 6.1, 7.7, 10.0\}$. We shall use parametrics

$$r_i = a \sin k(\theta_i - \theta_0) + b, \quad \theta \in [0, 2\pi], \quad (5.2)$$

to generate scatterers, where (r_i, θ_i) is the polar coordinates of \mathbf{r} with respect to given center \mathbf{c}_i . Here, two scatterers (see Fig. 5.4(a)) generated by (5.2) with $k = 2, a = 0.5, b = 1, \theta_0 = \frac{\pi}{4}$ and $\mathbf{c}_1 = (0, -1)$ and $\mathbf{c}_2 = (2, -3)$ are tested. Given incident wave $u^{\text{inc}} = e^{i(-\frac{3\sqrt{2}}{5}x - \frac{3\sqrt{2}}{5}y)}$, the scattering field u^s are plotted in Figs. 5.4(b) (real part) and 5.4(c) (imaginary part). In Table

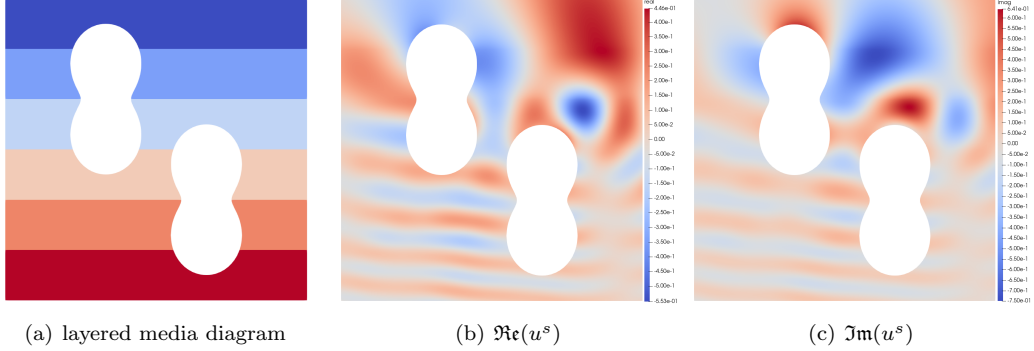


Figure 5.4: Problem diagram and numerical solution

5.2, the number of iterations and the total CPU time are presented. Further, the number of iterations and CPU time of the FMM accelerated iteration and the preconditioning in each iteration are plotted in Figs. 5.5 and 5.6. The results show that the preconditioning is very effective and the computational complexity of each iteration step is $\mathcal{O}(N)$.

Table 5.2: Iteration Steps and Iteration time

Elements	Iteration Steps	Iteration Steps with preconditioning	Time(sec)	Time(sec) with preconditioning
12000	93	59	1628.33	1362.33
24000	104	66	1822.82	1520.70
48000	115	72	2429.23	1685.44
96000	132	81	3042.68	2058.86
192000	162	93	3807.98	2827.82

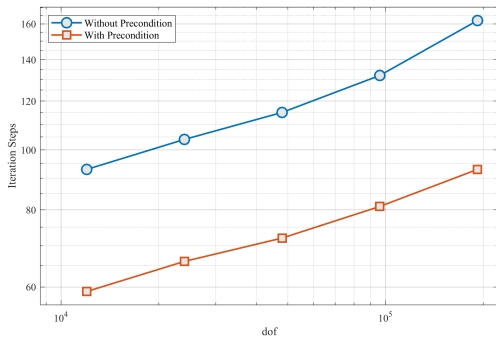


Figure 5.5: Iteration steps vs dof

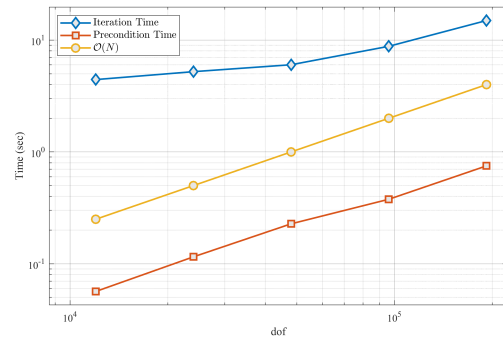


Figure 5.6: Time per iteration step vs dof

Example 3. Consider the layered medium of six layers with interfaces at $y = \{0, -1, -2, -3, -4\}$, where the reflection indices and the wave numbers are specified as $\eta = \{1, 2, 3, 4, 5, 6\}$ and $k = \{2, 3, 6, 5, 8, 10\}$. Five scatterers (see Fig. 5.7(a)) determined by (5.2) with $k = 5, a = 0.2, b = 0.7, \theta_0 = 0$ and $\mathbf{c}_1 = (-1.5, 0), \mathbf{c}_2 = (1.5, 0), \mathbf{c}_3 = (0, -2), \mathbf{c}_4 = (-1.5, -4)$ and $\mathbf{c}_5 = (1.5, 4)$ are tested. Given incident wave $u^{\text{inc}} = e^{-i2y}$, the scattering field u^s are plotted in Figs. 5.7(b) (real part) and 5.7(c) (imaginary part). The performance of the fast algorithm

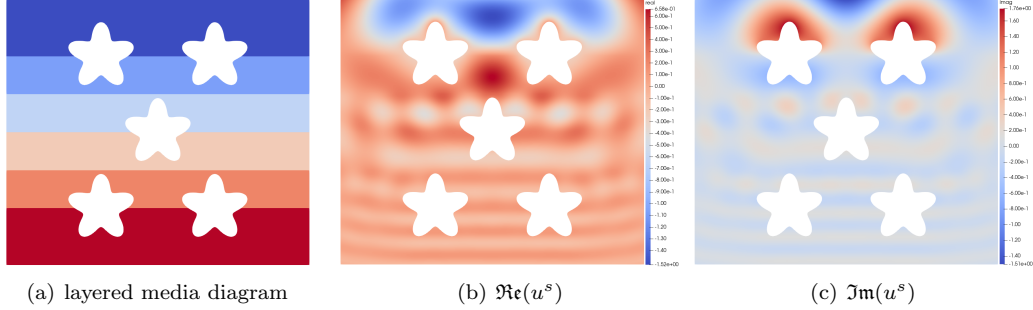


Figure 5.7: Problem diagram and numerical solution

is presented in Table 5.3, Fig. 5.8 and Fig. 5.9. Apparently, the same conclusion on the efficiency of the algorithm can be obtained as we have validated in Example 2.

Table 5.3: Iteration Steps and Iteration time

Elements	Iteration Steps	Iteration Steps with preconditioning	Time(sec)	Time(sec) with preconditioning
12000	125	71	1638.88	1553.62
24000	138	79	1742.52	1639.49
48000	156	88	2031.50	1831.76
96000	173	101	2708.44	2649.50
192000	192	112	3782.74	3056.38

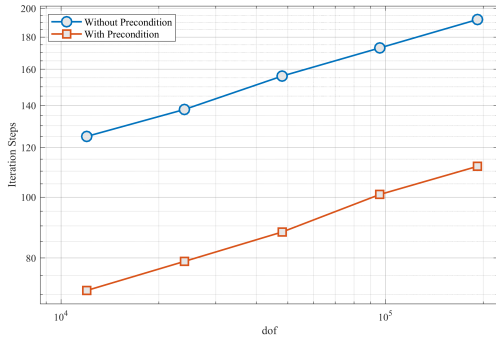


Figure 5.8: Iteration steps vs dof

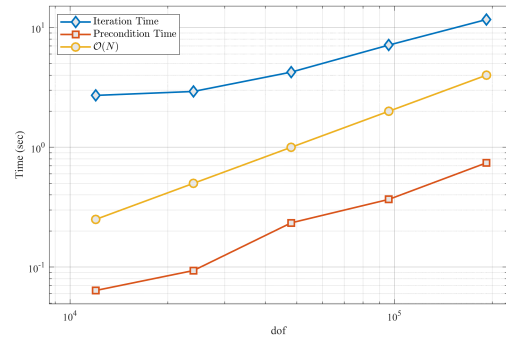


Figure 5.9: Time per iteration step vs dof

Conclusion and future work

In this paper, we have developed a FMM accelerated boundary integral method for solving two-dimensional Helmholtz equation for acoustic wave scattering problems in multi-layered media. By using the layered Green's functions to formulate the boundary integral equations, the interface transmission conditions are naturally satisfied without redundant unknowns and integral equations on the interfaces. The lowest order Nyström method is used to discretize the integral equation. An improved layered media FMM and an overlapped domain decomposition preconditioner are proposed to accelerate the matrix free GMRES iterative solver for the resulted dense linear system. A set of numerical experiments demonstrated the $\mathcal{O}(N)$ complexity and robustness of the method, confirming its capability for efficient scattering simulations in complex multilayer configurations.

For the future work, the extension of the present framework to three-dimensional layered media will be considered, where the complexity of Sommerfeld integrals and interface coupling poses additional challenges. Besides, further advances in preconditioning strategies and parallel implementations will be considered to enable large-scale simulations in high-frequency regimes.

Acknowledgment

The research of the first and second author is supported by NSFC (Grant No. 12022104 and 12371394). The research of the third author is support by the Major Program of Xiangjiang Laboratory(Grant No. 22XJ01013) and the Foundation Sciences of Hunan Province (Grant No. 2024JC0006). The research of W. Cai is supported by Clements Chair of Applied Mathematics at Southern Methodist University.

References

- [1] S. B. Naqvi, L. J. Ayton, Acoustic scattering by multi-layered gratings, *J. Sound Vib.* 610 (2025) 119083.
- [2] J. Ha, J. Shin, K. Lim, I.-K. Um, B. Yi, 3d uhr seismic and back-scattering analysis for seabed and ultra-shallow subsurface classification, *Acta Geophys.* 73 (2) (2025) 1363–1376.
- [3] M. Alibakhshikenari, B. S. Virdee, A. A. Althuwayb, S. Aïssa, C. H. See, R. A. Abd-Alhameed, F. Falcone, E. Limiti, Study on on-chip antenna design based on metamaterial-inspired and substrate-integrated waveguide properties for millimetre-wave and thz integrated-circuit applications, *J. Infrared Millim. Terahertz Waves* 42 (1) (2021) 17–28.
- [4] Z. Chen, W. Zheng, Pml method for electromagnetic scattering problem in a two-layer medium, *SIAM J. Numer. Anal.* 55 (4) (2017) 2050–2084.
- [5] X. Jiang, Y. Qi, J. Yuan, An adaptive finite element pml method for the acoustic scattering problems in layered media, *Commun. Comput. Phys.* 25 (1) (2019) 266–288.
- [6] H. Dastour, W. Liao, A fourth-order optimal finite difference scheme for the helmholtz equation with pml, *Comput. Math. Appl.* 78 (6) (2019) 2147–2165.
- [7] X. Jiang, X. Duan, A pml finite element method for electromagnetic scattering problems in a two-layer medium, *J. Sci. Comput.* 90 (1) (2022) 34.

- [8] B. Engquist, A. Majda, Absorbing boundary conditions for numerical simulation of waves, *Proc. Natl. Acad. Sci. U.S.A.* 74 (5) (1977) 1765–1766.
- [9] R. L. Higdon, Absorbing boundary conditions for acoustic and elastic waves in stratified media, *J. Comput. Phys.* 101 (2) (1992) 386–418.
- [10] M. Aksun, G. Dural, Comparative evaluation of absorbing boundary conditions using green's functions for layered media, *IEEE Trans. Antennas Propag.* 44 (2) (2002) 152–156.
- [11] L. Wu, M. Zhao, X. Du, A high-order absorbing boundary condition for scalar wave propagation simulation in viscoelastic multilayered medium, *Eng. Comput.* 38 (6) (2021) 2575–2603.
- [12] R. Kress, Boundary integral equations in time-harmonic acoustic scattering, *Math. Comput. Model.* 15 (3-5) (1991) 229–243.
- [13] A. Bendali, M. Fares, Boundary integral equations methods in acoustic scattering, *Computational Methods for Acoustics Problems* 1.
- [14] G. C. Hsiao, W. L. Wendland, Boundary integral equations, in: *Boundary Integral Equations*, Springer, 2021, pp. 25–94.
- [15] S. Zaman, A comprehensive review of boundary integral formulations of acoustic scattering problems, *Sultan Qaboos Univ. J. Sci.* 5 (2) (2000) 281–310.
- [16] A. Sommerfeld, Über die ausbreitung der wellen in der drahtlosen telegraphie, *Ann. Phys. (Berl.)* 333 (4) (1909) 665–736.
- [17] J. R. MOSIG, K. A. MICHALSKI, Sommerfeld integrals and their relation to the development of planar microwave devices, *IEEE J. Microw.* 1 (1) (2021) 470–480.
- [18] W. Hackbusch, *Hierarchical Matrices: Algorithms and Analysis*, Springer, 2015.
- [19] M. Bebendorf, Approximation of boundary element matrices, *Numerische Mathematik* 86 (4) (2000) 565–589.
- [20] E. Candès, L. Demanet, L. Ying, A fast butterfly algorithm for the computation of fourier integral operators, *Multiscale Model. Simul.* 7 (4) (2009) 1727–1750.
- [21] P.-G. Martinsson, V. Rokhlin, A fast direct solver for boundary integral equations in two dimensions, *J. Comput. Phys.* 205 (1) (2005) 1–23.
- [22] K. L. Ho, L. Greengard, A fast direct solver for structured linear systems by recursive skeletonization, *SIAM J. Sci. Comput.* 34 (5) (2012) A2507–A2532.
- [23] L. Greengard, V. Rokhlin, A fast algorithm for particle simulations, *J. Comput. Phys.* 73 (2) (1987) 325–348.
- [24] L. Ying, Fast algorithms for boundary integral equations, in: *Multiscale Modeling and Simulation in Science*, Springer, 2009, pp. 139–193.
- [25] B. Wang, W. Zhang, W. Cai, Fast multipole method for 3-d helmholtz equation in layered media, *SIAM J. Sci. Comput.* 41 (6) (2019) A3954–A3981.
- [26] W. Cai, T. Yu, Fast calculations of dyadic green's functions for electromagnetic scattering in a multilayered medium, *J. Comput. Phys.* 165 (1) (2000) 1–21.

- [27] K. A. Michalski, J. R. Mosig, Efficient computation of sommerfeld integral tails—methods and algorithms, *J. Electromagn. Waves Appl.* 30 (3) (2016) 281–317.
- [28] O. P. Bruno, M. Lyon, C. Pérez-Arcibia, C. Turc, Windowed green function method for the helmholtz equation in layered media, *SIAM J. Appl. Math.* 76 (5) (2016) 1871–1898.
- [29] G. Bao, W. Lu, T. Yin, L. Zhang, A highly accurate pml-bie solver for the electromagnetic scattering problem in a multilayered medium, *SIAM J. Sci. Comput.* 46 (6) (2024) A3849–A3872.
- [30] H. Wang, W. Lu, An fft-accelerated pml-bie solver for three-dimensional acoustic wave scattering in layered media, arXiv preprint arXiv:2412.11162.
- [31] W. Lu, L. Xu, T. Yin, L. Zhang, A highly accurate perfectly-matched-layer boundary integral equation solver for acoustic layered-medium problems, *SIAM J. Sci. Comput.* 45 (4) (2023) B523–B543.
- [32] J. Lai, L. Greengard, M. O’Neil, A new hybrid integral representation for frequency domain scattering in layered media, *Appl. Comput. Harmon. A.* 45 (2) (2018) 359–378.
- [33] J. Vanherck, B. Sorée, W. Magnus, Tanh-sinh quadrature for single and multiple integration using floating-point arithmetic, arXiv preprint arXiv:2007.15057.
- [34] W. Zhang, B. Wang, W. Cai, Exponential convergence for multipole and local expansions and their translations for sources in layered media 2-d acoustic wave, *SIAM J Numer. Anal.* 58 (3) (2020) 1440–1468.
- [35] H. Yuan, B. Wang, W. Zhang, W. Cai, Fast multipole method for maxwell’s equations in layered media, arXiv:2507.18491.
- [36] K. Nabors, S. Kim, J. White, Fast capacitance extraction of general three-dimensional structures, *IEEE Trans. Microw. Theory Tech.* 40 (7) (2002) 1496–1506.
- [37] W. C. Chew, *Waves and Fields in Inhomogenous Media*, John Wiley & Sons, 1999.
- [38] B. Wang, D. Chen, B. Zhang, W. Zhang, M. H. Cho, W. Cai, Taylor expansion based fast multipole method for 3-d helmholtz equations in layered media, *J. Comput. Phys.* 401 (2020) 109008.
- [39] W. Cai, *Deterministic, Stochastic, and Deep Learning Methods for Computational Electromagnetics*, Springer, 2025.
- [40] P. A. Martin, *Multiple scattering: interaction of time-harmonic waves with N obstacles*, no. 107, Cambridge University Press, 2006.
- [41] L. Ying, G. Biros, D. Zorin, A kernel-independent adaptive fast multipole algorithm in two and three dimensions, *J. Comput. Phys.* 196 (2004) 591–626.
- [42] K. Nabors, S. Kim, J. White, S. Senturia, Fast capacitance extraction of general three-dimensional structures, in: [1991 Proceedings] IEEE International Conference on Computer Design: VLSI in Computers and Processors, 1991, pp. 479–484.